COURSE

NEUTRINO ANOMALIES

Frank Sciulli †

Columbia University & Nevis Labs
Box 137
Irvington, NY 10533
USA

† e-mail: sciulli@nevis1.nevis.columbia.edu

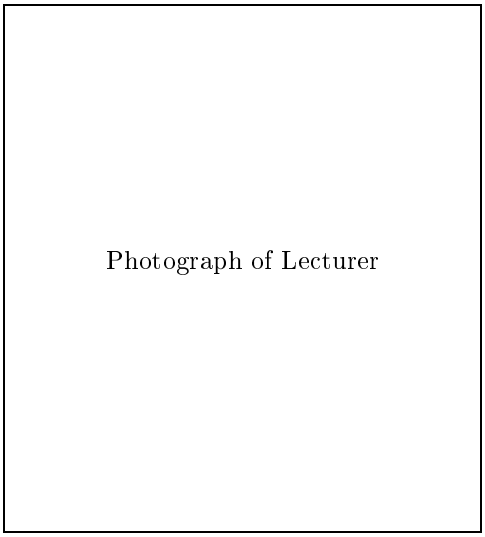
Photograph of Lecturer

Contents

1. Neutrino Properties

1.1. Introduction

These lectures are intended to introduce the essential concepts associated with neutrinos, and to describe some exciting and topical questions. To me, the most exciting issues are the three current positive indications for neutrino oscillations. My emphasis may shortchange many important experiments on neutrinos, and so I apologize up front.

First allow me to state that I am an experimentalist. Though I spent a considerable fraction of my professional life using neutrino beams, for the last several years I have worked at ZEUS (HERA) learning about the high energy electron-proton interaction. Perhaps this background qualifies me to be more objective in presenting neutrinos, though it hardly gives me more expertise on current issues. Hoping for more of the former than the latter, I state my frank opinion: the issue of neutrino mass is one of the most exciting discovery possibilities in elementary particles.

At the same time, let me state clearly that there is now no conclusive evidence that neutrinos have non-zero mass. There are several experimental anomalies, whose interpretations may ultimately be related to neutrino mass. The conclusive positive experiment (or experiments) to demonstrate neutrino mass is (are) still to be done. It is in large part this last statement that motivates these lectures: to motivate thought about experiments that could demonstrate mass and oscillations among neutrino states and to point the way to measurements of associated mass parameters and couplings.

1.2. Fundamental Properties

Fermion Families

Neutrinos were hypothesized in the early 1930's to account for the missing momentum associated with nuclear β-decay. Only in 1959 was the first direct observation of the neutrino interaction made. In the meantime, between 1937-47, the muon (μ) was discovered. Confusion about the μ during this decade was a consequence of the political distraction of a World War and the scientific distraction created by the predicted strongly-interacting

particle at nearly the same mass (π). As more information about muon decays subsequently accumulated, particularly the absence of the decay $\mu \to e + \gamma$, it became impossible to reconcile the muon as just a heavy electron: the muon needed to be a member of a lepton family distinct from the electron. This became the only tenable picture in 1964 when the muon neutrino (ν_μ), resulting from an accelerator-produced beam of decaying pions, was observed to produce muons (and not electrons) in its interactions. About ten years later, a third distinct lepton, the τ, was discovered. Though we have yet to observe direct interactions of initial state ν_τ, it is difficult to conceive how the tau-neutrino would *not* have the same weak interactions as the ν_e and the ν_μ. All evidence shows that these three neutrinos interact only through the left-handed weak interactions.

Though the masses of the *charged* leptons are finite (between 0.5 MeV and 2 GeV) and well-measured, *neutrino* masses are only bounded – by upper limits (in the worst case below 24 MeV and probably below about 40 eV). The known leptons are nicely grouped into three distinct families:

$$\begin{pmatrix} e^- \\ \nu_e \end{pmatrix} \qquad \begin{pmatrix} \mu^- \\ \nu_\mu \end{pmatrix} \qquad \begin{pmatrix} \tau^- \\ \nu_\tau \end{pmatrix} \tag{1.1}$$

While the leptons were being discovered, quarks were discovered to be fundamental constituents of protons. Together, quarks and leptons constitute the only known elementary fermion fields. The three separate families of quarks have now all been observed.

$$\begin{pmatrix} d \\ u \end{pmatrix} \qquad \begin{pmatrix} s \\ c \end{pmatrix} \qquad \begin{pmatrix} b \\ t \end{pmatrix} \tag{1.2}$$

The special characteristic of leptons is the absence of direct strong interactions. On the other hand, leptons couple to quarks (and to all hadrons) through the electroweak interaction carried by photons (γ) and weak bosons (Z^0, $W^\pm$). It is intriguing that just three families of each kind of matter have been found.

Even *more* intriguing is the fact that there are no more than three elementary left-handed neutrinos of low mass. The first measurement [1] of the full decay width of the Z^0 (and compared with Standard Model expectations) clearly showed that there are three and only three "unseen" decays involving $Z^0 \to \nu + \bar{\nu}$.* The number of families [2] obtained from the best current LEP measurements is 2.991 ± 0.016. There is simply no way to extend the families of (1.1) with more light, left-handed neutrinos.

* This limit on neutrino families was anticipated by earlier, less precise, cosmological arguments.

Neutrino Couplings

The couplings of neutrinos require the known microscopic world to be asymmetric! Since 1956, it has been known that the *charged current* Weak Interactions maximally violate parity. Neutrinos, with zero electric charge, also interact through *neutral* Weak Interactions with $V-A$ currents. For the small neutrino masses in evidence, as $v \to c$ only left-handed neutrinos (ν) interact and only right-handed antineutrinos ($\overline{\nu}$) interact. Is the world really so asymmetric? Or are the right-handed (RH) currents simply less obvious? It is possible that RH currents exist, but with more subtle manifestations. For example, rates for RH processes could be vanishingly small at presently available energies if the mass scale corresponding to the $V+A$ sector were much higher than the $V-A$ scale.

There are many ways to search for RH currents, both directly and indirectly. A very good review was done on this subject a few years ago[3]; there exist important constraints on the mixing and masses (M_N) of neutral leptons coupled to the RH sector. Coupling limits at very low masses ($M_N < 5\,MeV$) come primarily from nucleosynthesis constraints and observations of neutrinos from supernova SN1987A; at intermediate masses ($M_N < 50\,MeV$), from muon decay parameters; at higher masses from a variety of sources, with the neutral kaon mass difference playing a central role.

Even so, these limits do not obviate all possibilities. For example, searches for long-lived and/or heavy neutral leptons have been made in a variety of ways [4]. If evidence had been found for *any*, we would be discussing *that* today.

Neutrino Masses Directly Measured

Direct mass measurements of the neutrinos in (1.1) rely on the energy-momentum constraints for particles decaying into those neutrinos. The final state spectrum end-point is a sensitive measure of the neutrino mass square (m_ν^2), with sensitivity gauged by the reaction's energy release.* Table 1 gives limits, along with the reactions that provide those limits and the energy release.

Some time ago, there appeared tentative evidence of a finite mass value for the ν_e, but this situation has changed over the last decade. Table 2 provides mass measurements in this period [5] and includes two final entries from a more recent review [6]. Experiments give best fit end point

* Effectively experiments measure separately the energy (E) and momentum (p) of the lowest energy neutrinos, whose difference is $E - p \sim \frac{m_\nu^2}{2E}$.

Table 1
Reactions limiting neutrino masses.

Neutrino	Mass Limit	Reaction	Energy Release
Electron	10 eV	$^3H \rightarrow {}^3He + e^- + \nu_e$	18.6 keV
Muon	160 keV	$\pi^+ \rightarrow \mu^+ + \nu_\mu$	33 MeV
Tau	24 MeV	$\tau \rightarrow 5\pi(\pi^0) + \nu_\tau$	1700 MeV

parameters for the square of the electron neutrino mass, m_ν^2, which in many recent cases is negative. This clearly means that the model used to fit the spectrum and obtain the end point is not correct. Complete consensus has not been reached on resolving this issue, but problems associated with the atomic binding in the tritium molecule and the energy levels of the residual bound tritium-helium system could alter the spectrum near the end point, for example. Quoting an unambiguous mass limit in such circumstances is a bit flaky, perhaps, but the consensus is that neutrino masses above about 10 eV would show clear and observable effects [6]. Numerical limits[7] only moderately larger come from measurements of arrival times of neutrinos from the Supernova 1987A[8].

Table 2
Direct limits on electron neutrino masses.

Group	Year	Source	Best Fit m_ν^2 (eV^2)	Value/Limit
ITEP, Moscow	'88	Valine	$+676 \pm 235$	$= 26$ eV
Los Alamos	'91	gas	$-147 \pm 68 \pm 41$	≤ 9.3
Zurich	'91	OTS-T	$-24 \pm 48 \pm 61$	≤ 11
INS, Tokyo	'91	Cd A-T	$-65 \pm 85 \pm 65$	≤ 13
Mainz	'93	T solid	$-39 \pm 34 \pm 15$	≤ 7.2
LLNL	'94	T gas	$-130 \pm 20 \pm 15$	≤ 7
INR, Moscow	'94	T gas	-18.5 ± 6	≤ 4.5
Mainz	'96		$-22 \pm 17 \pm 14$	≤ 5.6
Troitsk	'96		$1.5 \pm 5.9 \pm 3.6$	≤ 3.9

Cosmological Neutrino Mass Limits

Direct upper limits on the second and third family neutrino masses are high. Indirect limits on all neutrino family masses arise from their expected cosmological abundances (similar to photons), and the fact that as the universe expands, the neutrinos can red-shift only as low as their rest mass

energies. Though it is deemed implausible [9] for neutrinos to make up all the "missing mass" in the universe, any stable neutrino mass in excess of a few eV would have a substantial effect on the cosmic density of matter and the resultant expansion rate. Denoting Ω_ν the critical density of neutrinos in the universe and h the Hubble parameter,

$$\Omega_\nu h^2 = \sum \frac{m_\nu}{93\,eV} \tag{1.3}$$

where the sum is over all three neutrino families. For the age and expansion rate, $\Omega_\nu h^2 \leq 0.4$, the limit [9] on the sum over the three neutrino family masses is

$$\sum_{families} m_\nu \leq 40\,eV \tag{1.4}$$

This limit is variously quoted between 20 and 100 eV, depending on assumptions.

The only reasonable escape from 1.4 requires at least one of the more massive neutrinos (like the ν_τ) to decay, since equation (1.4) applies only to stable neutrinos. Such a scheme has the difficulty that all such known decays would proceed much too slowly for the decays to have an effect on the limit. (This criticism can be avoided by requiring new particles or new interactions.) It appears unlikely that we will find *stable* neutrinos with masses in contradiction to a limit within a factor two of that required by equation (1.4).

Neutrinos *Could Be* Different - Dirac and Majorana

Since our subject is neutrino mass, let us *assume* that the neutrino fields have nonzero rest masses. Because neutrinos are electrically neutral, they may have different properties from all other elementary spin-1/2 fields [10]. Our intuitive picture has been conditioned by elementary *charged* fermions. The left-handed neutrino (ν_L) born in weak interactions, traveling at less than the speed of light, will be seen as a right-handed neutrino (ν_R) from *some* Lorentz frame. On the other hand, the state that arises from the CPT operation* on ν_L (the $\overline{\nu}_R$) can be distinct from either of these, just as the right-handed positron is distinct from both the left and right-handed electrons. If this is the case for neutrinos, its mass is said to be Dirac-like.

* CPT, the product of charge conjugation, parity, and time reversal substitutes the antiparticle state for the particle state. All legitimate field theories preserve CPT invariance.

Because neutrinos have no electric charge, it is possible that the states, $\overline{\nu}_R$ and ν_R, are the same. For this case, the neutrino is said to be Majorana-like. A Majorana neutrino is different from a Dirac neutrino! The process of viewing the Majorana neutrino from a different Lorentz frame would cause the neutrino to become an antineutrino! Indeed, it is possible for the neutrino to have either a Dirac- or a Majorana-mass, or both. It is up to experiment to decide which, among these possibilities, nature has chosen.

If the electron neutrino had a large Majorana mass, there are particularly sensitive ways to detect it. These are the so-called "neutrino-less double beta decays" ($\beta\beta_{0\nu}$):

$$\begin{array}{ll} \beta\beta_{2\nu} & A(Z,N) \rightarrow A(Z+2,N-2) + 2e^- + 2\overline{\nu}_e \\ \beta\beta_{0\nu} & A(Z,N) \rightarrow A(Z+2,N-2) + 2e^- \end{array} \tag{1.5}$$

The $\beta\beta_{2\nu}$ decay *must* arise from second-order weak charged current interactions. Such processes have now been observed in many nuclei, including ^{82}Se, ^{76}Ge, ^{100}Mo, and ^{150}Nd. The $\beta\beta_{0\nu}$ has not been seen, though there have been many intensive searches. A positive result would constitute direct confirmation of Majorana mass associated with the electron neutrino. The lifetime for such a process, after unfolding the relevant nuclear matrix elements, depends on the square of an effective mass parameter, M_{eff},

$$M_{eff} = \sum CP_i \left|L_{ei}\right|^2 m_i \tag{1.6}$$

so that the mass parameter depends on the CP phases, the appropriate matrix elements (L_{ei}) of the "lepton mixing matrix", and the Majorana masses (m_i) themselves. The limits from many experiments and many nuclei have been reviewed[11], with limits extending to below one eV. A recent limit, quoted at the Lepton-Photon conference in Hamburg [12] from the Heidelberg-Moscow group gives $M_{eff} < 0.5\,eV$. It would appear that even better limits are expected in the future.

Neutrinos Masses *Are* Different

Some of us grew up thinking of integer spin fields as force carriers and half-integer spin fields as matter, even though we did not know whether the neutrinos had mass or not. Present knowledge limits neutrino masses to much lower values than the other known matter fields. This is illustrated in figure 1, taken from the review by Raffelt[9]. The masses (or mass limits) are plotted for each of the elementary fermion types. The dashed lines connect the "families".*

* It should be noted that, though the lepton connections are established by lepton flavor

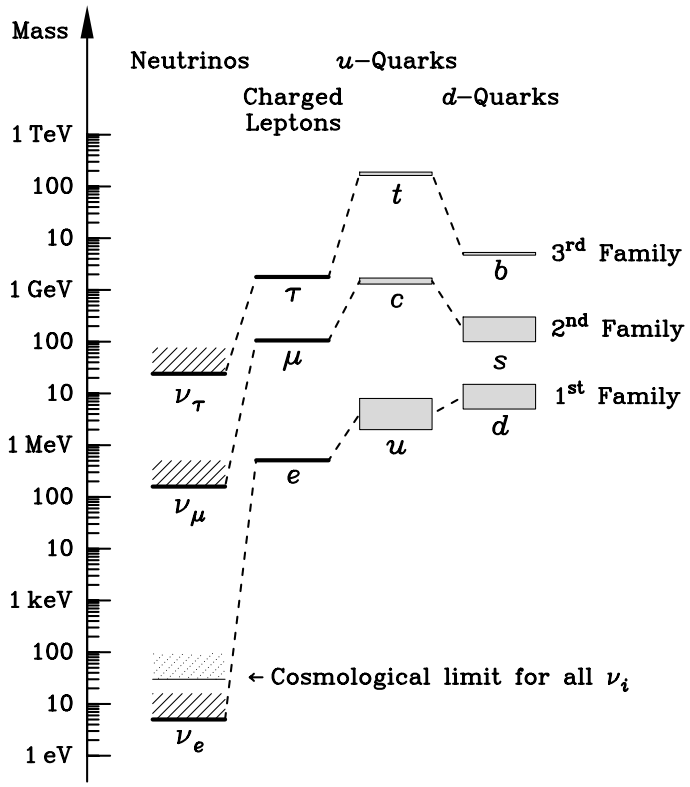

Fig. 1. Mass or mass limits of the several elementary fermions.

The most interesting feature of figure 1 is that the present *direct* limits on neutrino masses are at least two orders of magnitude smaller than the corresponding charged lepton and quark masses. Assuming the cosmological mass limit (equation 1.4) applies to all neutrino types, the ν_τ mass is at least *seven* orders of magnitude smaller than the charged counterparts. By comparison, differences among the charged fermion family members

conservation and the quark connections are established by the largest terms in the weak interaction quark (CKM) mixing matrix, the connections of lepton to quark families have no such rationale. Hence, these connections should be viewed as an assumption, motivated by mass-ordering.

are generally less than two orders of magnitude. Figure 1 demonstrates clearly that nature has made the neutrino mass uniquely small. Perhaps the masses are identically zero, reflecting an exact $V-A$ structure to weak forces. But, it is also very possible that neutrino masses are finite but tiny, and these small masses are related to the kinds of mass – Majorana as well as Dirac – available to neutral leptons. I obviously find the latter alternative more attractive.

Origins of Mass in a Fermion Family - "See-saw mechanism"

The much smaller neutrino masses could be a consequence of two factors: (1) The neutrinos have both Dirac and Majorana mass in contrast to the charged fermions with only Dirac mass. (2) New interactions like the missing right-handed weak interaction – and the new bosons and fermions associated with them – may be part of nature, but only visible at much higher energies.

In our usual picture of the Electroweak interaction, exact gauge symmetry requires the fermions to have zero mass; mass is acquired by the fermions (with I=$\frac{1}{2}$) because of symmetry-breaking induced by the Higgs boson (also I=$\frac{1}{2}$). In this picture, the known charged fermions acquire a mass proportional to the Higgs vacuum expectation, $\langle\phi\rangle$:

$$m \simeq h_V \langle\phi\rangle \simeq \frac{1}{\sqrt{G_F}} \simeq 250\ GeV \tag{1.7}$$

where G_F is the Fermi constant. It is anticipated that any new interactions (like right handed weak currents) will unify with the electroweak at a very high energy scale. For convenience, let us refer to this new high scale as the GUT scale. Fundamental particles there will have masses, M_{GUT}, somewhere between TeV energies and the Planck mass, $\mathcal{O}(10^{16}$ GeV). For definiteness, let's illustrate with a measure comfortably out of present-day reach like $M_{GUT} \simeq 10^{15}\,GeV$, so that the ratio of scales is of order $m/M_{GUT} \sim 10^{-13}$.

Also for definiteness, assume that the right-handed weak interaction emerges at this high mass scale with a force carrier, $W_R^{\pm}$, and a "right-handed neutrino", N_R. In contrast to the charged lepton (l^-) and the associated neutrino (ν) which cohabit an isodoublet, we further assume the new right-handed neutrino (N) to be alone in an isosinglet*. Presumably the "natural" Dirac mass scale for the left-handed sector is given by equation 1.7, whereas the natural mass scale for the N is more like M_{GUT}.

* These very specific assumptions are for illustration. Other assumptions, for example about the isospin structure, also lead to the qualitative see-saw features.

Because both ν and N are neutral and massive, their left- and right-handed components may in general couple. The Lagrangian reflecting this is of the form [10,13]:

$$\left(\begin{array}{cc} \overline{\nu}_L & \overline{N^c}_L \end{array} \right) \left(\begin{array}{cc} m_T & m_D \\ m_D & m_S \end{array} \right) \left(\begin{array}{c} \nu^c_R \\ N_R \end{array} \right) \tag{1.8}$$

The off diagonal terms in this matrix are Dirac-mass terms and the diagonal terms are Majorana-mass terms. Furthermore, the isospin change induced by each is shown in table 3.

Table 3
Isospin properties of the mass terms in expression 1.8.

	ΔI	term
m_T	1	isotriplet Majorana
m_D	$\frac{1}{2}$	isodoublet Dirac
m_S	0	isoscalar Majorana

But these isospin properties determine the magnitudes of the matrix elements in equation (1.8). We have already seen that the Dirac scale $m_D \sim m$ of equation (1.7), since the Higgs field is an isodoublet. Similar dimensional arguments require the triplet mass to be

$$m_T \sim h_V \frac{\langle \phi \rangle^2}{M_{GUT}}$$

in order to preserve the isospin properties with the available mass scales. Conversely, the isoscalar mass has nothing to do with the Higgs sector, so

$$m_S \sim M_{GUT}$$

Hence equation (1.8) incorporates an isodoublet Dirac mass term (m_D) of order the charged fermion mass, but the isotriplet mass term (m_T) could be 10^{-13} times smaller. And the isosinglet mass term (m_S) could be 10^{+13} times larger. Ignoring the smaller of these, the mass matrix (from expression 1.8) becomes

$$\left(\begin{array}{cc} 0 & m \\ m & M_{GUT} \end{array} \right)$$

with eigenvalues (labeled for convenience by N and ν)

$$\begin{aligned} m_N &= M_{GUT} \\ m_\nu &= \frac{m^2}{M_{GUT}} \end{aligned} \tag{1.9}$$

Fortunately, we end with the mass of the (presently unobserved) right-handed neutrino (M_N) high enough so that it would not have been observed thus far. But the second term is also important: the neutrino member of each family obtains a mass (m_ν) smaller than those of charged fermions by a factor of $\frac{m}{M_{GUT}}$, a number which might be as small as 10^{-13}. This feature provides a natural mechanism by which the neutrinos can have much smaller masses than the charged counterparts – how tiny depends on the value of M_{GUT}. The neutrino could be lighter by a few to as many as thirteen orders-of-magnitude.

Three Families and Conclusions

The above argument motivates a Lagrangian describing the Majorana-Dirac neutrino (equation 1.8) as a 2×2 matrix for a single family. But the real world has three families of leptons, requiring a 6×6 matrix. Some off-diagonal components of this matrix connect our familiar neutrinos to unseen, or "sterile" neutrinos. But other elements connect familiar neutrinos of one family with familiar neutrinos in another. There is therefore ample opportunity and a reasonable context, if nature has chosen to make such components nonzero, to have mixing among neutrino families. (There is also opportunity for any neutrino to mix with sterile counterparts in its own or another family.)

Though there is no evidence requiring neutrinos to have mass, there is no compelling argument for the mass to be identically zero.* The neutrino is sister to the charged leptons and quarks. Comparing neutrinos with these other fermion fields, *massless* neutrinos would seem truly exceptional. On the other hand, there is ample evidence that neutrino masses are at least several orders of magnitude smaller than their charged brothers.

The see-saw mechanism provides a reasonable context in which to reconcile this puzzle. We have chosen a specific illustrative example which results in a "quadratic see-saw" (equation 1.9). Other mechanisms can produce a linear relationship[14]. Most higher symmetries with right-handed sectors have these general features: (a) smaller neutrino masses than the charged fermions; (b) different masses for neutrinos of different families; and (c)

* The zero mass photon is related to the absolute conservation of electric charge; what absolute principle would zero mass neutrinos provide – aside from some exact nature of the $V - A$ interaction?

couplings among the families which would produce lepton flavor violation at some level. If the world is like this, there must exist (at some level) the phenomenon of "Neutrino Oscillations". We describe such possibilities in section 3. In the meantime, we describe an anomaly which may be related to oscillations - the Solar Neutrino Problem.

2. The Solar Neutrino Problem

2.1. Introduction

A long-standing and still unresolved problem concerns the paucity of electron neutrinos (ν_e) coming from the core of the Sun. We believe we know the mechanisms by which the Sun produces energy; there are inescapable consequences for how many neutrinos are produced by the same mechanisms. The several versions of the "Standard Solar Model" (SSM) give predictions which generally agree among themselves. Experiments measuring neutrino fluxes at the Earth, however, do not agree with the SSM predictions. There is now little doubt that neutrinos of several different energies are fewer than calculated in any reasonable model for solar energy production. In this section we discuss the predictions and the evidence.

2.2. Solar Production of Heat and Neutrinos

The energy that feeds the Earth emanates from the Solar surface, at a black body temperature of about 5000K. Roughly ten thousand years earlier, that energy was created deep in the core, where the temperature is about 15×10^6K. The three major fusion cycles providing this energy, shown in table 4, also produce electron neutrinos (ν_e). For example, each *pp* cycle turns four protons into a single ^4He nucleus along with 26.7 MeV energy, two positrons, and two neutrinos. The *pp* neutrino energies inhabit a continuum up to about 0.42 MeV. The dominant source of energy seen at the surface is the *pp* cycle. Fluxes of more energetic neutrinos (like ^7Be and ^8B in table 4) are usually dependent on ingredients produced in earlier cycles.* Relationships between radiant energy and neutrino flux are calculable so long as the thermodynamic properties of the Sun (temperature, density, etc.) are understood and the energy dependent cross sections are known.

* A more complete inventory of neutrino flux cycles is shown in figure 2. Though important to the self-consistency of the solar flux calculation, those not given in table 4 are neither major producers of neutrinos observed in experiments nor of the radiant energy at the surface.

Table 4
Major fusion cycles in the solar furnace.

Cycles	Reactions
pp	$p + p \rightarrow {}^2H + e^+ + \nu_e$ ${}^2H + p \rightarrow {}^3He + \gamma$ ${}^3He + {}^3He \rightarrow {}^4He + p + p$
${}^7Be$	${}^3He + {}^4He \rightarrow {}^7Be + \gamma$ $e^- + {}^7Be \rightarrow {}^7Li + \nu_e$ ${}^7Li + p \rightarrow {}^4He + {}^4He$
${}^8B$	$p + {}^7Be \rightarrow {}^8B + \gamma$ ${}^8B \rightarrow {}^8Be^* + e^+ + \nu_e$ ${}^8Be^* \rightarrow {}^4He + {}^4He$

Assuming the Sun does not change in any substantial way over periods like $10,000$ years, the presently well-measured surface luminosity provides severe constraints on the predicted number of neutrinos produced in the core.

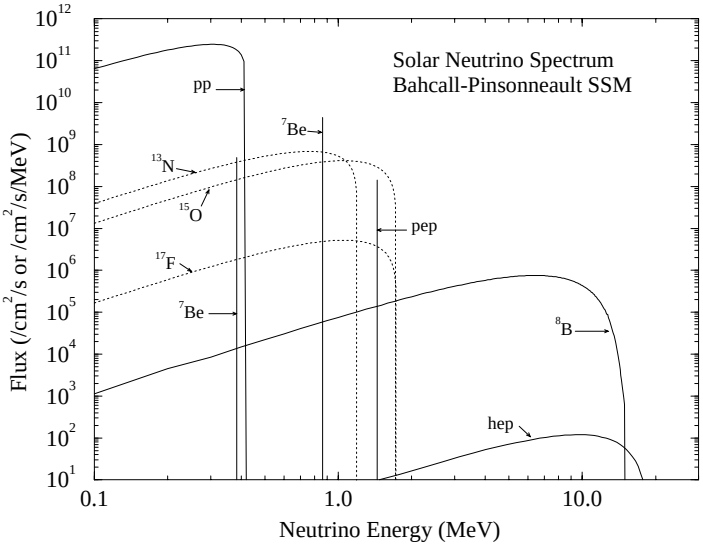

Fig. 2. The energy dependence of the Solar neutrino flux.

Predictions for the neutrino flux spectra are illustrated[15] in figure 2. The flux spectrum is such that, as we go from higher to lower energies, the neutrinos from the ^8B cycle first dominate ($E_\nu > 2$ MeV). When the threshold drops to $E_\nu > 0.8$ MeV, the ^7Be neutrinos become more important. For $E_\nu < 0.4$ MeV, the *pp* cycle dominates.

2.3. Solar Neutrino Experiments

Table 5 shows [16] the reactions and threshold energies for each of the five experiments* which have observed the solar neutrino flux. They are described below and more fully in the quoted references. The detected reactions, along with the energy threshold required to trigger this process are shown. The last column gives a recently quoted rate relative to one (BP) theoretical calculation [17].

Table 5

Experiments measuring solar neutrino flux. See text.

Experiment	Type	Reaction	Threshold	Exp/Theory
Homestake	Rad-chem	$\nu_e + {}^{37}Cl \rightarrow e^- + {}^{37}Ar$	0.8 Mev	0.273±0.021
SAGE	Rad-chem	$\nu_e + {}^{71}Ga \rightarrow e^- + {}^{71}Ge$	0.23 MeV	0.504±0.089
GALLEX	Rad-chem	$\nu_e + {}^{71}Ga \rightarrow e^- + {}^{71}Ge$	0.23 MeV	0.509±0.059
Kamiokande	Part. Det.	$\nu_e + e^- \rightarrow \nu_e + e^-$	7.3 MeV	0.423±0.058
SuperKamio.	Part. Det.	$\nu_e + e^- \rightarrow \nu_e + e^-$	7.3 MeV	0.379 ±0.034

The very important feature of these experiments is that *all* observe (last column) far fewer neutrinos than expected. We briefly review the experiments.

Homestake Experiment

Homestake, the first and longest operating solar neutrino experiment, used as target 615 tons of perchloroethylene (C_2Cl_4), a chemical with commercial use as cleaning fluid [18,19]. The threshold energy for the detected reaction is such that the dominant rate should be from ^8B neutrinos

* The SuperKamiokande result given in this table is for 100 days of operation. Preliminary data given in figure 3 is for 200 days of operation. Information was provided at the recent 1997 Lepton-Photon conference for 300 days of running. Note that the raw units traditionally used for the radiochemical experiments is "SNU", or solar neutrino units defined as 10^{-36} interactions per atom per second. Kamiokande collaborations quote results in flux units of 10^6 per cm^2 per second.

($\sim 75\%$), and most of the remainder from ^7Be neutrinos. The experiment operated for nearly thirty years beginning in 1967 at the Homestake mine in South Dakota. The gaseous Ar was removed monthly by Helium purge, passed through various condensors, sieves, traps, and filters and finally separated from the Cl atoms with gas chromatography. The subsequent decay electron from $^{37}Ar \rightarrow {}^{37}Cl + e^+ + \nu_e$, with a half-life of 35 days, was observed with a proportional counter. The signal level averaged 0.48 events per day, whereas the background (from cosmic rays) was about 0.06 per day. On the basis of the solar model, roughly 1.5 events per day were expected. Results over thirty years of operation have consistently indicated many fewer solar neutrinos than expected.

SAGE and GALLEX Experiments

The gallium experiments [18] [20], like Homestake, use radiochemical techniques. Unlike Homestake, the energy threshold is low and the major rate contributor is the *pp* cycle. The GALLEX experiment, located in the Gran Sasso underground laboratory, uses 12 tons of ^{71}Ga (in 30 tons of gallium) as represented in 100 tons of $GaCl$. SAGE, conceptually similar, is operated by a Russian-American collaboration in the underground laboratory at the Baksan Valley, Caucasus. The experiment uses 57 tons of metallic gallium. Again a complex series of extraction and counting processes are performed to periodically separate nuclei which have made the transition to ^{71}Ge. Both experiments have calibrated the efficiencies of their detectors with approximately ten percent precision and the two experiments have consistent results – roughly half the rate predicted by the SSM.

Kamiokande and Super Kamiokande

Neutrinos from the Sun have been observed by direct particle detection. The Kamiokande experiment [21] did this first; recent results have come from the newly commissioned Super Kamiokande experiment[22]. These real-time "Water Ĉerenkov" experiments each utilize a large water-filled tank instrumented with photomultipliers to observe the final state electron in the elastic process of table 5.* Final-state relativistic particles emit Ĉerenkov light into photomultipliers (PMTs) spread over a surface within

* This elastic process can occur with neutrino flavors other than electron – through the NC Z^0-exchange. The rates in the Ĉerenkov detectors from such processes are smaller by a factor of about six. The fits to oscillation hypotheses described later take these NC reactions into account.

the tank walls and pointed inward. Other PMTs point outward to provide signals of particles that create light near the tank edges. The detectors are located in Japan at a depth of 2700 meters of water equivalent (mwe). Observing electrons from neutrinos with energies as low as several MeV in real time was a *tour-de-force*.

The original Kamiokande experiment was designed to search for proton decay; a similar detector (IMB) operated at about the same time – beginning in 1983 – and both set important limits on proton decay rates. Neutrinos from the famous supernova (SN1987A) were observed [23] by both experiments. A new, much more massive, SuperKamiokande detector began operating in 1996. A comparison between the physical characteristics of the old and new Kamiokande detectors is given in Table 6.

Table 6
Reactions limiting neutrino masses.

	Kamiokande	Super Kamiokande
Total Mass	3,000 tons	50,000 tons
Fiducial Mass	680 tons	22,000 tons
Solar Threshold	7.3 MeV	5 MeV
Solar Rate	1 per week	160 per week
PMT diameter	50 cm	50 cm
Number PMT	1,000	12,000

A unique capability of such "real-time experiments" provides the direction of the final electron from $\nu_e + e^- \to \nu_e + e^-$. Kamiokande saw a signal of these electrons which points on average to the Sun. SuperKamiokande has verified the rate and the directionality. Figure 3 shows recent data [24] from early operation of SuperKamiokande; the polar angle peak in the direction of the Sun demonstrates the unambiguous presence of solar neutrinos. We return later in this section to discuss additional questions that real-time experiments can answer on the Solar neutrino issue.

2.4. Comparisons with Solar Models

The measured solar neutrino rates from all the experiments are well below the calculated predictions. Where two experiments are sensitive to neutrinos of comparable energies, they give consistent answers. It is highly unlikely that all the experiments in table 5 are wrong. Experiments sensitive to different neutrino energies, however, do not obtain precisely the same answer. Figure 4, from a 1994 review of the subject [25], shows the

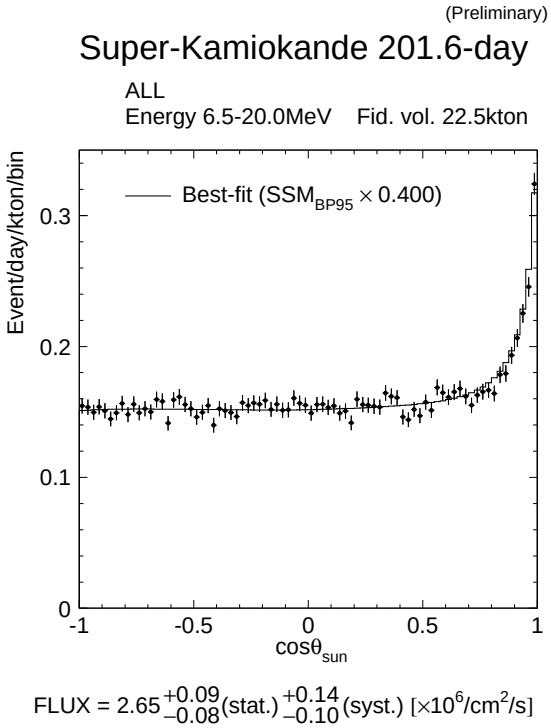

Fig. 3. The direction, relative to the Sun, associated with the charged final state observed from low energy neutrino interactions. The flat region corresponds to random background; the peak near $\cos\theta = 1$ corresponds to the signal from the Sun.

ratio of the experimental rates to the predictions (for two different flux calculations) plotted versus energy.

The Homestake experiment (Cl), with an intermediate threshold energy, shows less relative flux than the other two types of experiments. (Dependence on energy will be important if neutrino oscillations are relevant to the interpretation, since energy dependence sets a mass scale.) Unfortunately, Homestake is the only experiment which has not yet been corroborated. Improved precision for the Gallium and Ĉerenkov experiments is clearly also important.

Figure 4 also allows us to compare two different Solar Models [17,26]. Though there are differences in predictions and estimated uncertainties, they are not nearly large enough to account for the serious discrepancies between experiment and prediction.

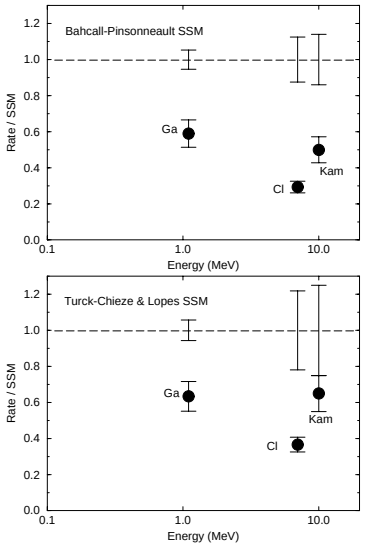

Fig. 4. Apparent energy dependence of the ratio of observed to expected neutrino flux for two different flux calculations. The "Cl" label refers to the Homestake experiment. The "Kam" point is primarily sensitive to B-cycle neutrinos, "Cl" to the Be-cycle, and "Ga" to the pp-cycle.

Be assured, uncertainties in the input parameters associated with the solar neutrino predictions *are* important. The neutrino production rates depend on the cross-sections for the processes of table 4, which in turn depend strongly on energy – and therefore on the solar core temperature. However, unless there is some inexplicable solar time variation (on the scale of 10,000 years) the visible luminosity at the surface – which primarily arises from the pp cycle – severely constrains (both from above and below) the neutrino fluxes. The fluxes from some cycles can be modified at the expense of others within the model. For example, the ^7Be and ^8B fluxes can be reduced relative to the pp flux by lowering the core temperature. But such a modification *must* reduce the higher energy ^8B flux *more* than the ^7Be flux. This contrasts with the feature seen in figure 4: the measured flux appears to be *larger* at the higher energy. This feature is a natural consequence of flavor oscillations, as we will discuss in section 3.

Measuring Interior Temperatures of Sun

A very interesting relatively recent development [27] confirming the good

knowledge of the Sun's energy production, involves measurements[28] of the speed of sound deep within the Sun. These follow from measurements of the frequency-dependent power spectrum for sound waves at the solar surface. There is a strong correlation between the wave frequency and the radius at which waves are initiated. By transforming the sound distributions, appropriately weighted, the sound velocity versus radius from the solar center is obtained. Since the square of sound velocity at any given radius is proportional to pressure over density, this quantity therefore depends on solar temperature divided by density. Measurements agree with solar models in which helium and metal diffusion are taken into account, but disagree (at about the two percent level) with models which do not include diffusion. Though these measurements primarily test our knowledge at radii larger than about 1/3 the solar radius (whereas the neutrinos are created deeper in the core), the agreement even into small radii [27] can only instill confidence in the calculations and in the thermodynamic solar properties used in those calculations.

Model-Independent Analyses

Of course, a solar model incorporates many different assumptions, some fundamental, some not. Since any measurement requires a paradigm in which to describe it, it is not possible to fit observations of neutrinos with no assumptions. However, assumptions can be relaxed in order to understand sensitivities. This has been done [16,25] with the flux normalizations for the most important cycles (*pp*, ^7Be, and ^8B of table 4) left as parameters. The overall flux normalization [$\phi(pp)+ \phi(^7Be) + \phi(^8B)$] is severely constrained by the visible surface luminosity, so the two remaining normalization parameters were chosen to be $\phi(^7Be)$ and $\phi(^8B)$, relative to their SSM predictions.

Figure 5, using data in hand as of May 1997, shows probability contours required by the data at several confidence levels. The SSM with associated uncertainty is indicated in the upper right hand corner. The figure shows clearly that the data prefer little, even negative, flux from ^7Be, simultaneous with less than half that expected from ^8B. This of course makes no sense for many reasons, especially since the ^8B-neutrinos rely on adequate numbers of ^7Be nuclei made (with ^7Be neutrinos) in the ^7Be cycle. (See table 4.)

The dots at the upper right show the effects of varying parameters of the SSM within errors, and the other symbols show the effects of assuming major departures from the SSM: assumptions not in evidence otherwise for either the Sun or for particles/cosmology. Such assumptions (none of

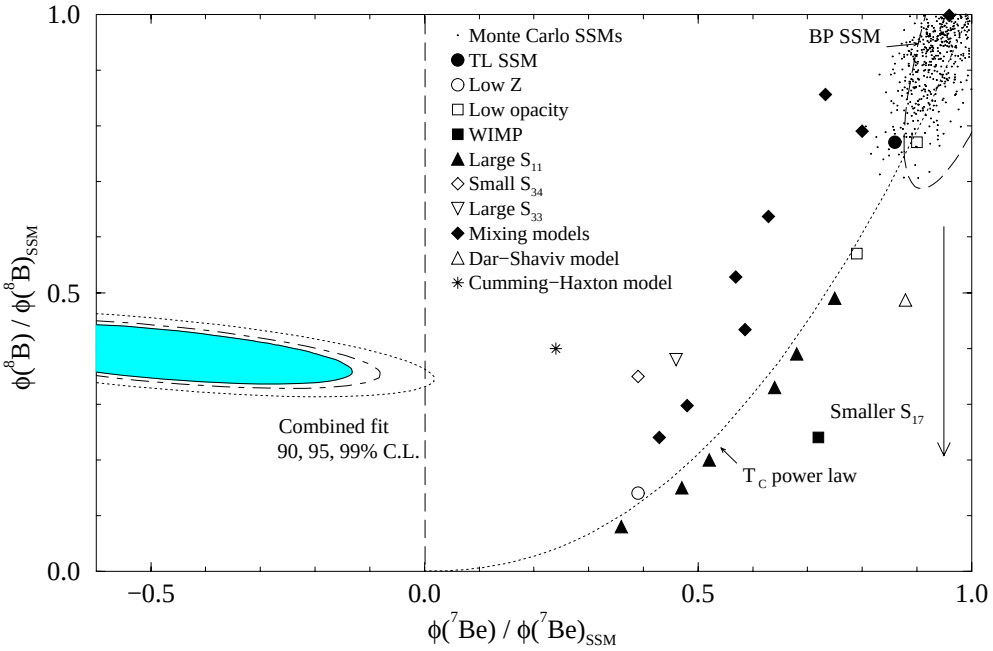

Fig. 5. Fit [16] of available data to best values of flux normalizations as described in the text.

which involve neutrino oscillations) give a range of possible values for the parameters (in which, for example, ^7Be flux almost always decreases faster than the ^8B flux). This is not like the parameters required by the data: $\phi(^7Be)$ less than 7% that required in the SSM and $\phi(^8B)/\phi_{SSM}(^8B) = 0.41 \pm 0.04$.

Real-time Measurements

The Kamiokande/SuperKamiokande experiments permit event-by-event measurements of energy and time, as well as the directional information (figure 3). These permit additional comparisons to see if other anomalies are apparent. For example, the Kamiokande data [29] as a function of observed energy has been compared with SSM expectations. The data with energies $E > 7$ MeV, are consistent with lying a fixed factor below SSM predictions.

Additional comparisons likewise provide no clues. It has been known for

some time that the number of sunspots on the solar surface varies with a cycle of about a decade. The neutrino data show no variation over such a period. No day/night variations have been seen: any such variation must be at the ten percent level or lower. (Though no dependences are seen, these results are important in delineating possible parameters for a neutrino oscillation interpretation.) The recent Super Kamiokande [22] data have also been examined for such features. Thus far, with statistical precision similar to Kamiokande, conclusions are qualitatively similar. With the large improvement in fiducial mass and much observation time remaining, more information will be likely in the future.

2.5. Conclusions

Table 7
Summary of Solar Anomaly.

	Threshold	Ratio to BP SSM
SAGE/Gallex	0.23 MeV	0.507 ± 0.049
Homestake	0.8 MeV	0.273 ± 0.021
Kamiokande/Super K	7.3 MeV	0.391 ± 0.029

Five experiments show substantial disagreement between measured neutrino flux and predictions from the Standard Solar Model. The three different parts of the sampled neutrino spectrum are given in table 7. These show clearly the anomaly: substantially less solar neutrino flux is observed at the Earth than expected. The data also indicate that the effect is energy dependent. A very attractive explanation is oscillation of the neutrino leptonic flavor into other flavors – μ, τ, or sterile. We discuss these next.

3. Oscillations

3.1. Introduction

The idea of oscillating states is an essential element of Quantum Mechanics. The neutral K-meson system taught us that such states could be specified by discrete quantum numbers describing internal properties like "strangeness". For the kaon, the eigenstates produced in the strong interactions are the $K^0 - \overline{K}^0$ (particle and antiparticle) strangeness states; the subsequent propagation and decay of the kaon, on the other hand, define "weak interaction" mass eigenstates, $K_S^0 - K_L^0$ of mixed strangeness

but almost conserving particle-antiparticle (CP) symmetry. In the neutrino sector, production takes place through the weak interactions which conserve lepton flavor. But the mass eigenstates which subsequently propagate are defined by the overall Lagrangian which could have different flavor properties, as discussed in section 1.

3.2. Two-component Oscillations

For illustration, consider the two state system consisting of the electron-type $|\nu_e\rangle$ and some other neutrino state $|\nu_x\rangle$ which could be the muon, tau, or some other as yet unknown "sterile" type. The mass *eigenstates*, $|\nu_1\rangle$ and $|\nu_2\rangle$, can be different; the mixing between base states is parameterized by an angle, θ, and the relationship between the bases is the 2×2 rotation matrix:

$$\begin{pmatrix} |\nu_e\rangle \\ |\nu_x\rangle \end{pmatrix} = \begin{pmatrix} \cos\theta & \sin\theta \\ -\sin\theta & \cos\theta \end{pmatrix} \begin{pmatrix} |\nu_1\rangle \\ |\nu_2\rangle \end{pmatrix} \tag{3.1}$$

For neutrinos made by nuclear reactions in the Sun, the $|\nu_e\rangle$ state is produced. Consider an initially pure electron neutrino beam, $|\nu(0)\rangle = |\nu_e\rangle$, made with momentum p; the time-dependent state is

$$|\nu(t)\rangle = |\nu_1\rangle \cos\theta \exp[-iE_1 t] + |\nu_2\rangle \sin\theta \exp[-iE_2 t] \tag{3.2}$$

where E_i are the energies of the mass eigenstates. The amplitude to find the neutrino in the x-state at a later time, t, is

$$\langle \nu_x \mid \nu(t)\rangle = -i \sin(2\theta) \sin\left(\frac{E_2 - E_1}{2} t\right) \tag{3.3}$$

Since we are interested in neutrino *masses* at the electron volt level or less and *energies* above the kilovolt level, the neutrinos are relativistic: it is in general a good approximation to replace $E_i = p_i + \frac{m_i^2}{2E_i}$, so that

$$\begin{aligned} E_2 - E_1 &= \tfrac{\Delta m^2}{2E} \\ \Delta m^2 &= m_2^2 - m_1^2 \end{aligned} \tag{3.4}$$

The probability to find the state $|\nu_x\rangle$ a distance $L = ct$ from the production of a $|\nu_e\rangle$ is

$$P(\nu_e \to \nu_x) = \sin^2(2\theta) \sin^2\left[\frac{\Delta m^2 L}{4E}\right] \tag{3.5}$$

After supplying the usual dimensional factors (Planck's constant and velocity of light), and with units expressed

$$\begin{array}{ll} \Delta m^2 & \text{in eV}^2 \\ L & \text{in meters (or kilometers)} \\ E & \text{in MeV (or GeV)} \end{array} \tag{3.6}$$

formula (3.5) becomes

$$\begin{aligned} P(\nu_e \to \nu_x) &= \sin^2(2\theta) \sin^2\left[1.27\tfrac{\Delta m^2 L}{E}\right] \\ P(\nu_e \to \nu_e) &= 1 - P(\nu_e \to \nu_x) \end{aligned} \tag{3.7}$$

3.3. Judging Experiments

Equation (3.7) may be examined to get a sense of scale and to estimate the parameter space an experiment might explore. For example, for $\Delta m^2 = 1$ eV^2, the probability reaches its first maximum with $E = 1$ MeV neutrinos at $L = 0.79$ meters; for 1 GeV neutrinos at 0.79 kilometers.

An experiment in which oscillations are *not* observed, with specific average values of L and E, will limit the probability, $P(\nu_1 \to \nu_2) \leq \delta$. This limit places coupled constraints on the parameters, Δm^2 and $\sin^2(2\theta)$. An illustrative example, shown in figure 6, is the limit placed by the CCFR experiment [30] which used initial muon neutrinos with energies near 100 GeV and oscillation paths of order 1 kilometer. The limit contour shown in figure 6 excludes values of the parameters to the right and above the contour.

At very *large* values of Δm^2, the oscillating argument changes so quickly that finite resolutions in energy and/or position allow us to replace the argument by its average, $\sin^2\left[1.27\frac{\Delta m^2 L}{E}\right] \sim 1/2$. At the other extreme, for the mixing sensitivity near unity and the mass parameter small, the sine is well approximated by its argument. These give the following limiting cases

$$\begin{array}{lll} \text{large } \Delta m^2 & & \sin^2 2\theta < 2\delta \\ \text{large } \sin^2 2\theta & \Delta m^2 < \frac{E}{1.3L}\sqrt{\delta} & \end{array} \tag{3.8}$$

The figure illustrates the case where the probability is limited to $P < .001$ at the 90% confidence level (CL). Between the two extremes in equation (3.8), the contour limits depend on details like resolution and statistics of the experiment.

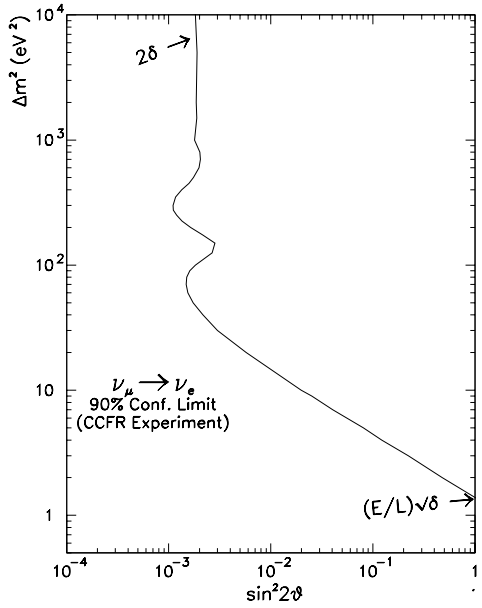

Fig. 6. Illustration of the limits on two-component oscillation parameters obtained from the CCFR experiment.

3.4. Solar Anomaly as Vacuum Oscillations

As discussed in the last section, the observed solar neutrino flux is low by a factor of two. If the neutrinos are created as anticipated, observations indicate that those neutrinos do not arrive intact at the Earth. One possible explanation is that lepton flavor oscillations are responsible. Pursuant to this, we apply equations 3.7, appropriate to 2-component oscillations for the $L = 1.5 \times 10^{11}$m space between locations. Because the observed effect is so large, the mixing parameter would need to be $\sin^2 2\theta \sim 1$. Given that the anomaly appears up to the highest energy neutrinos, $E < 10$ MeV, the vacuum oscillation (for argument near $\pi/2$) must have mass parameter, Δm^2, near a value 10^{-10} eV^2. If there were no energy dependence in the data, Δm^2 could be much larger than this value (corresponding to many oscillations over the intervening space); conversely if there is energy dependence in the observations (as there appears to be), then $\Delta m^2 \sim 10^{-10}$ eV^2. The fits [16] to all the solar data shown in figure 7 are quite acceptable ($\chi^2 = 9.9$ for 9 DOF). The optimal values, $\Delta m^2 = (5 - 8) \times 10^{-11}$ eV^2 and $\sin^2 2\theta = (0.65 - 1.0)$, are in the range anticipated above.

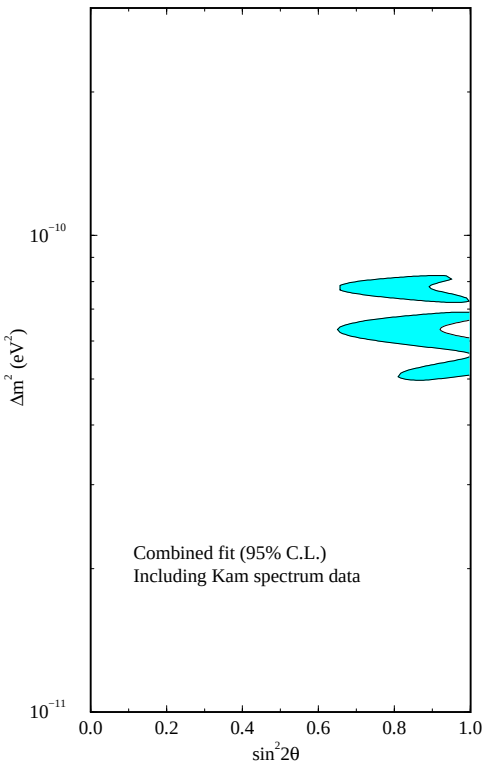

Fig. 7. Fit to hypothesis of vacuum oscillations, using the rate data from all the Solar neutrino experiments, as well as the spectrum from the Kamiokande experiment.

Vacuum oscillations constitute a logically possible resolution to the solar neutrino deficit: the hypothesis is consistent with present data. However if oscillations exist, it is not the *only* possibility. We discuss in the next section an oscillation in which the parameters are very different from those above.

3.5. Neutrino Flavor Regeneration - MSW Effect

Our analogy to neutrino flavor oscillation, used in section 3.1, was the neutral kaon system. Recall that a pure K^0 beam, after the short-lived component decays away, leaves the K^0_L eigenstate. This consists (ignoring the small CP-violating component) of half K^0 and half $\overline{K^0}$. When such

a beam passes through matter, the equilibrium is disrupted because the particle and antiparticle components interact at different rates: the forward scattering amplitudes are different and K_S^0 must again appear.

A similar "regeneration" phenomenon, called "MSW" for the inventors [31], should be expected under appropriate conditions if neutrino flavors mix. For neutrinos traversing matter, the ν_e component interacts differently from the ν_x component, no matter whether x corresponds to the μ, τ, or sterile. The ν_e has a unique charged current interaction with electrons, involving t-channel exchange of a $W^{\pm}$. This amplitude does not contribute to the cross-section for any other neutrino flavor.*

The time development of such a state is described by a 2×2 matrix, for which all components depend on the intrinsic mixing parameters and the diagonal components depend in addition on the weak interaction coupling, G_F, and the electron density, n, in the local region traversed by the neutrino. The mixing is complete when the diagonal components become identically zero, a resonance condition met† when the electron density is

$$n_{res} = \frac{1}{\sqrt{2}G_F} \frac{\Delta m^2}{2E} \cos(2\theta)$$

If the neutrino passes through a region of this density, the neutrino must completely flip its flavor identity. There are two important differences between vacuum oscillations and matter oscillations:

(i) The parameter space in MSW oscillations does not depend on the distance, L, between source and observation but only on having passed through a region of appropriate electron density, $n = n_{res}$.

(ii) In two component vacuum oscillations, some phase information is lost because of finite resolutions in energy and distance. The probability to flip cannot get smaller than 1/2 if all phase information is lost. By contrast an electron neutrino, after passing through a region with $n = n_{res}$, can have zero probability to remain an electron neutrino.

* For the sterile case, the neutral current cross-section is also different. We only discuss the non-sterile case, or "active flavors" here. See reference [32].

† We discuss here adiabatic transitions. Also not discussed here are different cases like antineutrinos passing through an electron medium, for which there will be no MSW oscillations (with $\Delta m^2 > 0$). For discussion of more general situations, see for example reference [33].

3.6. Solar Anomaly as MSW Oscillation

As outlined in an early discussion [32] of the MSW phenomenon, electron densities in the Sun and the neutrino energy spectra dictate that solar oscillations would occur for mass parameters in the range $10^{-10} \leq \Delta m^2 \leq 10^{-4}\, eV^2$. A recent fit [16] for ν_e oscillating to "active" neutrinos is shown in figure 8.

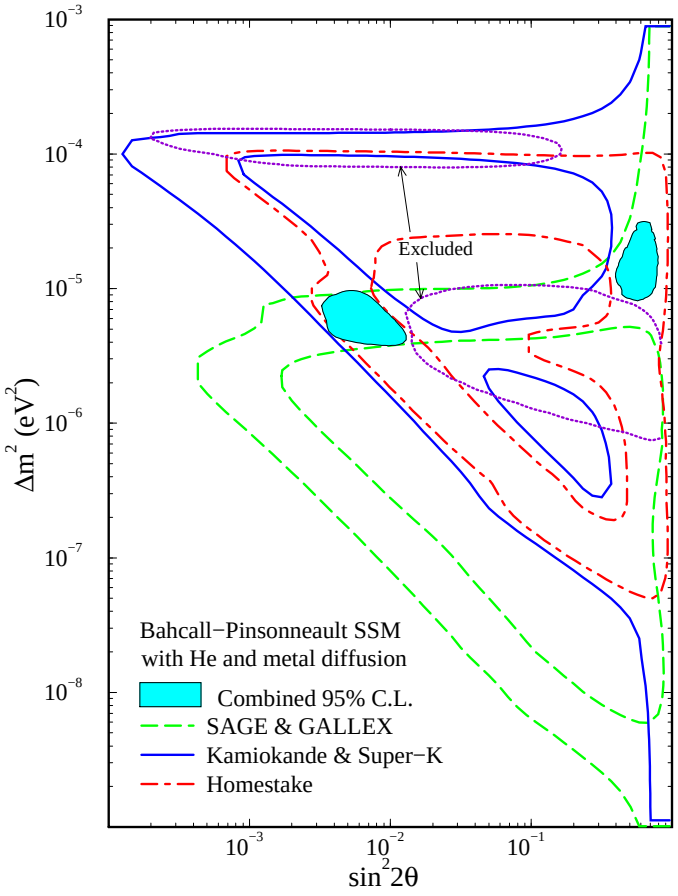

Fig. 8. Fit to the MSW solutions for all relevant Solar neutrino data, including the rate results from all three experiment types, spectrum data from Kamiokande, and the day-night rates from Kamiokande. The last two provide the exclusion regions indicated. See text and reference [16].

Table 8
Solutions to oscillation hypothesis using solar data.

	Sterile Neutrino		Active Neutrino	
	Small	Large	Small	Large
$\sin^2 2\theta$	1.0×10^{-2}	0.72	8.2×10^{-3}	0.63
$\Delta m^2\,(eV^2)$	4.0×10^{-6}	8.9×10^{-6}	5.1×10^{-6}	1.6×10^{-5}
χ^2 (7 DOF)	6.7	13.7	5.9	6.3

The three experimental rates delimit the interior portions of the parameter space indicated by solid, dashed, and dash-dot contours. Additional regions are excluded based on limits in (a) variation in the Kamiokande energy spectra (upper excluded region) and (b) variation in the Kamiokande day-night rates (lower excluded region)*.

Note the triangular shapes of the contours set by the rate limits. The severe limits extending to small values of $\sin^2 2\theta$ at high $\Delta m^2 \sim 10^{-4}\,eV^2$ corresponds to resonant densities near the Solar core. As Δm^2 decreases, the resonance would occur further from the core and the limit on $\sin^2 2\theta$ becomes weaker. As Δm^2 gets even smaller, resonance would require densities lower than the electron density at the solar surface. Though the several limit contours for different experiments have the same general shape, the contour from one experiment is translated in Δm^2 by an amount that scales with the experiment's mean energy sensitivity. The best fits define two discrete regions (shaded) permitted by all experiments, described as the "small angle" and "large angle" solutions.

Table 8 gives the best fit oscillation parameters for the active neutrino case, as well as for the sterile neutrino case. All have acceptable values of χ^2, though the large angle sterile case is not as good. As data gets better, some or all may become unacceptable.

3.7. More Flavor Components

Though we have concentrated on the two component case for pedagogical reasons, the ideas can be extrapolated to three or more components[34]. There *are* three familiar flavors, and there might be additional sterile flavors. However, the mathematics quickly becomes complicated as the number of components increases. With more than two flavors, the CP phases

* The density of electrons in the earth is sufficient to produce visible MSW oscillations for the specified region of $\Delta m^2 - \sin^2 2\theta$.

become important. The requirements of invariance under CP and CPT are

$$\begin{aligned} CP: &\quad P(\nu_\alpha \to \nu_\beta) = P(\overline{\nu_\beta} \to \overline{\nu_\alpha}) \\ CPT: &\quad P(\nu_\alpha \to \nu_\beta) = P(\overline{\nu_\alpha} \to \overline{\nu_\beta}) \end{aligned}$$

For n flavors ordered in eigenstate masses, $m_1 < m_2 < m_3 < ... < m_n$, the familiar flavor states (labeled with Greek characters) may be expressed as linear combinations of the mass eigenstates (labeled with Arabic characters)

$$\nu_\alpha = \sum_{k=1}^{n} U_{\alpha k}\, \nu_k$$

so that the probability for observing the state β when the initial state was α is

$$P_{\alpha\to\beta} = \left| \sum_k U_{\alpha k}\, U^*_{\beta k}\, \exp\left(-i \frac{\Delta m^2_{k1} L}{2E}\right) \right|^2$$

For the case of only three flavor generations, there are but three masses (m_i) and three mass parameters (Δm^2) that enter, and the constraint

$$\Delta m^2_{12} + \Delta m^2_{23} + \Delta m^2_{31} = 0$$

must apply. Hence, if we imagine only oscillations among the three known flavors, there can be only two independent mass parameters. Furthermore, if one is very large – at least one other must also be large. This is important in discussing the several hints of oscillation: there is a limit to how many different ranges of mass parameter can be correct if we are limited to the three known flavors.

4. Atmospheric Neutrinos

4.1. Introduction

Energetic cosmic rays bombard our atmosphere continuously, producing neutrinos of muon (ν_μ) and electron (ν_e) types. Several experiments, particularly those using Water Ĉerenkov detectors (IMB, Kamiokande, and Super Kamiokande), have reported relative rates of muon and electron neutrino interactions inconsistent with expectations. This is an ongoing and potentially important issue: a possible indication of neutrino oscillations. If so, the mass parameter is different from that indicated by the Solar neutrino anomaly.

4.2. Source and Detection of Neutrinos

The atmosphere, extending upward about 10 km, is constantly bombarded from space by high energy protons and heavier nuclei. Interactions in the upper regions produce mesons (mostly pions), which decay through the chain (for the positive pion)

$$\pi^+ \to \mu^+ + \nu_\mu$$
$$\mu^+ \to e^+ + \nu_e + \bar{\nu}_\mu$$

A similar chain for the negative pion produces a $\bar{\nu}_\mu$, ν_μ, and $\bar{\nu}_e$. In either case, so long as both π and μ decay, two muon type neutrinos and one electron type neutrino result. The neutrinos easily penetrate the atmosphere, and even the Earth; a few will interact in massive detectors. The energy range of interest extends up from a few hundred MeV.

There are several independent calculations of neutrino flux [35–37] which differ in specific assumptions like the primary cosmic spectrum (falling roughly like $E^{-2.7}$), geomagnetic cutoffs, and heavy nuclear effects. The predicted fluxes differ[38] from calculation to calculation by 20 to 30%. However, the calculated *ratios* of generic ν_μ flux to ν_e flux differ by only about 5%. The data disagree with all the calculations by much more than this.

Detectors measure neutrino flux by observing charged current processes containing either an electron or muon in the final states. In order to compensate for detector dependence, comparisons with flux expectations use a double ratio of the form

$$R = \frac{\left(\frac{\nu_\mu}{\nu_e}\right)_{data}}{\left(\frac{\nu_\mu}{\nu_e}\right)_{MC}} \tag{4.1}$$

where the numerator describes the ratio of muon events to electron events and the denominator is the expected ratio for that detector and cuts using a Monte Carlo calculation*.

Two general detector types have been employed to this task. (In no case are final state electric charges observed, and so neutrinos are not distinguished from antineutrinos.) The first are the water Ĉerenkov detectors, which we have discussed earlier as Solar neutrino detectors. (The neutrinos of interest here are at much higher energies.) Such detectors include the

* Additional detector effects involving separation of the ν_μ and ν_e events require that the quantity R', defined later, actually be used.

IMB, Kamiokande, and SuperKamiokande experiments. The neutrino interactions occur inside the detectors (verified by absence of a signal in the veto array). The technique permits separation of events with an electron (which showers) from events with a muon (which traverses long distances without interaction). Final state electrons and muons are relativistic so Ĉerenkov radiation is emitted. The Ĉerenkov rings impinging at the detector surface appear qualitatively different for electrons (open ring with high energy density–"shower" appearance) relative to rings created by muons (filled ring with smaller energy density–"track" appearance).† Measurements by the photomultipliers (PMTs) of time and energy permit reconstruction of the neutrino interaction coordinates, charged lepton direction, and time of the event.

Other detectors (Frejus, NUSEX, Soudan2) use massive, segmented targets with tracking capabilities. For example, the Frejus detector[39] contains a fine grained 900 ton calorimeter with iron plates, flash tubes and Geiger tubes. The topologies of showering high energy electrons are very different from those of penetrating muons. Frejus accumulated data between 1984 and 1988.

Events in Kamiokande with all final state particles contained within the detector are designated "contained events", as contrasted with "partially contained events" (or "multi-GeV"), respectively. The visible energy of contained events is typically below 1.33 GeV. (Clearly, this geometrical division is different for the much larger SuperKamiokande experiment.) In addition, events are selected with interaction vertex outside the detector but whose muon stops in the detector ("stopping muons"), and events with final state muon passing completely through the detector ("through-going muons"). The calculated ν_μ spectra [38] are shown for these categories in figure 9.

4.3. Experimental Anomaly

Rates of μ-like and e-like events

The effect is best illustrated by the numbers of contained events shown in table 9 and described in the Kamiokande publication[40].

A large fraction of μ-like events are observed to decay, whereas a much smaller fraction of e-like events do so. This and the fact that these fractions are reproduced by calculations give confidence that the selections do as expected. The numbers shown in the last two columns reflect expectations

† Events with more than one ring are classified separately. These are expected since particles and showers in the hadronic debris can sometimes create a second ring.

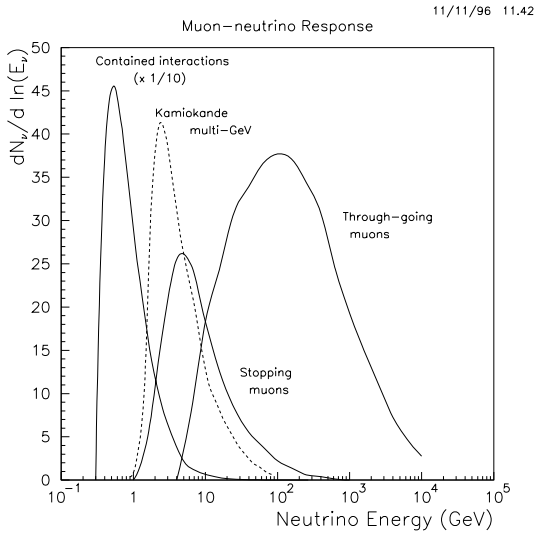

Fig. 9. Calculated flux spectrum for the various categories of events from the Kamiokande experiment described in the text. Note that the ordinate is the number of events per logarithmic interval of energy.

Table 9
Numbers of contained events described by Kamiokande.

Event	Data		Monte Carlo	
	Total	Decay	Total	Decay
Single Ring	482	182	584 (396)	270 (301)
μ-ring	234	158	357 (396)	248 (276)
e-ring	248	24	228 (257)	23 (25)
Multi-ring	208	82	234 (254)	94 (101)
Total	690	264	818 (907)	365 (402)

from the HKHM [36] flux calculations (upper values) and the BGS [35] flux calculations (lower values in parentheses), respectively. Though differences appear in the absolute predictions, there is a perceptible trend in the data relative to either calculation: the numbers of observed electron neutrinos

Table 10
Experiments measuring atmospheric neutrinos (1995).

Experiment	Exposure	R' (1995)
IMB-1	3.8 kton-yr	0.68 ± 0.08
Kamiokande ring	7.7	$0.60 \pm 0.06 \pm 0.05$
Kamiokande decay		$0.69 \pm 0.06 \pm 0.05$
IMB-3 ring	7.7	$0.54 \pm 0.05 \pm 0.05$
IMB-3 decay		$0.64 \pm 0.07 \pm 0.07$
Frejus contained	2.0	$0.87 \pm 0.13 \pm 0.07$
Soudan	1.0	$0.64 \pm 0.17 \pm 0.09$
NUSEX	0.5	0.99 ± 0.29

roughly correspond to expectations while the numbers of observed muon neutrinos do not.

The parameter quoted by experiments takes into account detector effects in separating μ-like from e-like events by using

$$R' = \frac{\left(\frac{\text{track}}{\text{shower}}\right)_{data}}{\left(\frac{\text{track}}{\text{shower}}\right)_{MC}}$$

The experimental ratios as reviewed in 1995 [13] are shown in Table 10.

Statistical (first) and systematic (second) errors on R' are shown. Note that the muon decay detection technique is independent, but such events are subsets of those in the row above; hence the events in the two categories are strongly correlated. The values range between $0.6 - 0.7$, except for Frejus and NUSEX, which had larger errors.*

This question was re-visited[41] in 1996 when there were a few changes in the list. The Frejus data, including all energies, was $R'_{Frejus} = 1.00 \pm 0.15 \pm 0.08$, in poor agreement with an anomaly. Since then, the Soudan experiment completed their analysis, giving $R'_{Soudan} = 0.72 \pm 0.19^{+\,0.05}_{-\,0.07}$. Overall, the Kamiokande experiment sees an effect of order three standard deviations (SD) from expectations, the IMB sees a two SD effect, Soudan about a one SD effect. On the other hand, Frejus and NUSEX (latter with large error) see no anomaly. A more recent result from Frejus [42] on upward-going high energy muons and electrons is also not in good agreement with an oscillation hypothesis.

* It should be noted that the Frejus collaboration [39] prefers not to have their data viewed this way; rather they include events of all energies. In that case, discussed later, their result is even less consistent with the anomaly.

Zenith angle dependence

Another tantalizing positive result came in the 1994 Kamiokande publication [40], reporting on the "multi-GeV" sample, which includes partially-contained events. The 98 electron-like events in this sample were largely contained whereas the 135 muon-like events were largely not. The observed value, $R' = 0.57 \pm 0.08$, is inconsistent with unity and consistent with the anomaly seen at lower energies.

The energies in this sample are high enough so that the correlation is strong between the final state lepton direction and the direction of the incident neutrino. The double ratio plotted versus zenith angle is shown in figure 10. For isotropic neutrinos made in the atmosphere all around the Earth and arriving unchanged at the detector, this distribution would be flat. The distribution of data in figure 10 does *not* appear flat, though the statistical argument for variation *around the average* is not compelling. For $\cos\theta = 1$, the neutrinos are produced overhead and so the distance traveled is about $L = 10$ km; for $\cos\theta = -1$, the neutrinos travel from the other side of the globe, so $L \simeq 10,000$ km. Demonstration of a strong dependence on zenith angle would be further, and strong, evidence for neutrino oscillations.

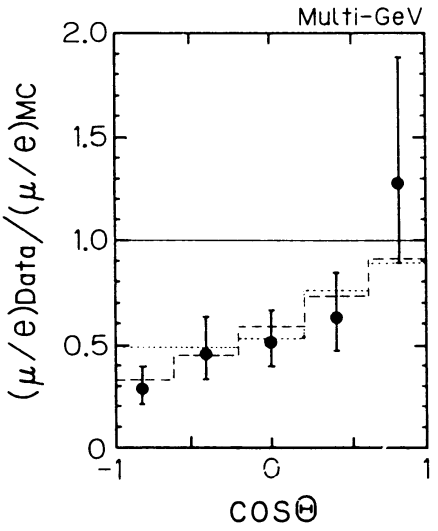

Fig. 10. The zenith angle distribution for Kamiokande multi-GeV events.

While this result adds excitement to the prospects for observing oscillations, the variation with zenith angle is of itself about a two standard deviation effect. More precision is required to conclude that the zenith angle dependence of atmospheric neutrinos constitutes another anomaly. To demonstrate neutrino oscillations would require even more.

4.4. Oscillation Interpretation

Interpretation of the atmospheric anomaly as two component neutrino oscillations leads to the parameter space delineated in figure 11. The shaded region shows the best fit to all 1994 Kamiokande data [40]. Note that the rates alone do not define an upper Δm^2 limit; the multi-GeV zenith angle dependence was required to specify this. The other curves on these plots are limits from Frejus, Gosgen, and CDHS. Note that the lowest, and most restrictive, curve is the Frejus [39] limit, which is not in good agreement with the Kamiokande conclusion.

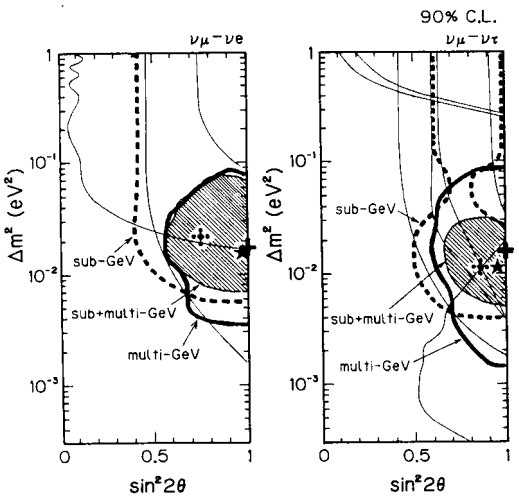

Fig. 11. Best fit values for the oscillation parameters [40] determined by the data associated with the atmospheric neutrino deficit. The left figure parameterizes the $\nu_\mu \to \nu_e$ hypothesis. The right figure parameterizes the $\nu_\mu \to \nu_\tau$ hypothesis.

4.5. New Data and Conclusions

The SuperKamiokande collaboration began to accumulate data in 1996 with more than an order of magnitude more fiducial volume than previous detectors. Data is being accumulated as we speak; results have been described at various times in 1997. The current values of R', including SuperKamiokande data from 200 days of operation[24], are summarized in table 11.

Table 11
Updated measurements (1997) of atmospheric neutrino ratios.

Experiment	R'
Kamiokande sub-GeV	$0.60 \pm 0.07 \pm 0.05$
Super K sub-GeV	$0.64 \pm 0.043 \pm 0.059$
Kamiokande multi GeV	$0.57 \pm 0.08 \pm 0.07$
SuperK multi GeV	$0.54 \pm 0.072 \pm 0.071$
IMB	$0.54 \pm 0.05 \pm 0.12$
Frejus	$1.00 \pm 0.15 \pm 0.08$
NUSEX	0.99 ± 0.29
Soudan 2	$0.72 \pm 0.19 \pm 0.06$

Though there are mixed results in this list, particularly the contrary result by Frejus, the remainder provide some consensus for an anomaly in the number of muon neutrinos relative to electron neutrinos. It cannot be ignored that the strongest effects come from water-Ĉerenkov detectors. The new SuperKamiokande results, however, are already non-trivial verifications of the anomaly. Many issues of experimental concern, like subtle differences in fiducial volume for electrons and muons, should be smaller (or at least different) in a detector more than an order of magnitude larger and with superior active coverage around the perimeter.

An anomaly exists in the number of muon versus electron atmospheric neutrinos observed by most experiments. However, demonstrating that this anomaly represents an oscillation phenomenon is a more difficult issue. Such an earth-shaking new phenomenon will require several observations, with differing conditions, of reproducible effects due to single values for the mixing and mass parameters. The zenith angle dependence is a candidate to provide a step toward such a demonstration. For two component oscillations as source of the anomaly, the zenith angle distribution at fixed neutrino energy would need R' to go from small to large values as $\cos\theta$ goes from -1 to 1. The value of zenith angle ($\cos\theta_t$) at this transition provides

the value of Δm^2. For differing neutrino energies, this transition region would need to shift in a predictable way. We hope the SuperKamiokande data will ultimately provide this kind of evidence.

In the meantime, it is encouraging that the average values of R' from SuperKamiokande reproduce the earlier experiments. Future data will be enormously interesting. In the end, this region of parameter space should be accessible to accelerator-based long baseline experiments. We discuss this later.

5. The LSND Anomaly

5.1. Introduction

Of the three anomalies sometimes interpreted as indicating neutrino oscillations, only one arises from an accelerator-based experiment. The "Liquid Scintillator Neutrino Detector" (LSND) at Los Alamos National Laboratory in New Mexico has observed final state positrons [43,44] from interactions of particles created as $\bar{\nu}_\mu$: 22 such events were found while only 4.6 background events were expected. We discuss this anomaly here.

5.2. LSND Detector

The Los Alamos Meson Facility (LAMF) produces 800 MeV protons at high current and dumps these into a high power beam dump. This proton energy is too low to make kaons. Most π^- are absorbed before decaying; the π^+ decay at rest. The production and decay chain is

$$\begin{aligned} p + N &\rightarrow N + N + \pi^+ \\ \pi^+ &\rightarrow \mu^+ + \nu_\mu \\ \mu^+ &\rightarrow e^+ + \nu_e + \bar{\nu}_\mu \end{aligned} \tag{5.1}$$

Note that there are no $\bar{\nu}_e$ in the decay products; these are smaller by a factor of 10^{-3} or less because of the smaller π^- production and the high likelihood for negative pions (and muons) to be absorbed. The neutrino spectrum includes the singularity of ν_μ at 30 MeV from two body pion decay, and the Michel spectrum with end point at 53 MeV for the ν_e and $\bar{\nu}_\mu$ from muon decay. (See equations 5.1.) These spectra are well understood; the overall normalization in the experiment is known to about 7%. Figure 12 shows the production region relative to the detector including the 30 meter propagation space for the neutrinos.

The detector [45] consists of 167 tons of liquid scintillator mixed with mineral water. The principle nuclei in the target are hydrogen and carbon

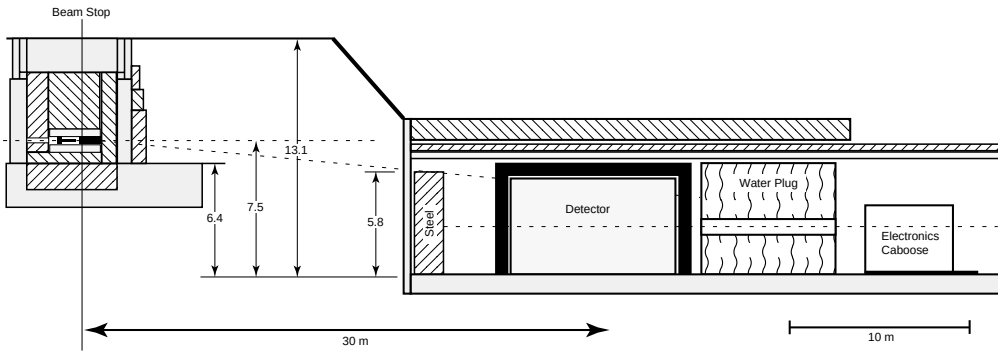

Fig. 12. The LSND beam line, consisting of the target region for the 800 GeV protons at the upper left and the neutrino detector as labeled.

($H/C = 2.05$); contaminations by nitrogen, oxygen, or other elements are small ($N/C = 3 \times 10^{-6}$ and $O/C = 1.5 \times 10^{-6}$). The detection processes are

$$\begin{aligned} \bar{\nu}_e + p &\rightarrow e^+ + n \\ n + p &\rightarrow d + \gamma \end{aligned} \tag{5.2}$$

with the positron observed promptly and the 2.2 MeV photon arising within the following 0.25 millisecond.

The clever idea that makes this experiment work is that the neutrino flavors created in the production target (equation 5.1) cannot easily provide the signature (equation 5.2). The muon neutrinos cannot make a μ, since the energies are well below threshold. The ν_e cannot make an electron from a proton (charge conservation), and the most likely background process, $\nu_e + {}^{12}C \rightarrow e^+ + {}^{12}N$, has a known cross section and small rate in this target. Even so, when this reaction *does* occur, the mass difference between ${}^{12}C$ and ${}^{12}N$ require the positrons to have energies below 36 MeV. Positrons above this energy are used to signal reaction (5.2).

Figure 13 shows the LSND detector geometry and PMT coverage. The inner surface of the vessel has 25% area coverage with 8 inch photomultipliers pointing inward. A veto system around the exterior covers the cylindrical sides and top. After the 1993 run, eighteen additional plastic scintillators were added along part of the bottom edge of the detector. The mineral is doped with adequate scintillator to obtain comparable amounts of scintillation light (which is isotropic) and Ĉerenkov light (emitted only by relativistic particles in a forward cone). The very large number of stopping muons in the detector permit reliable and continuous calibration with

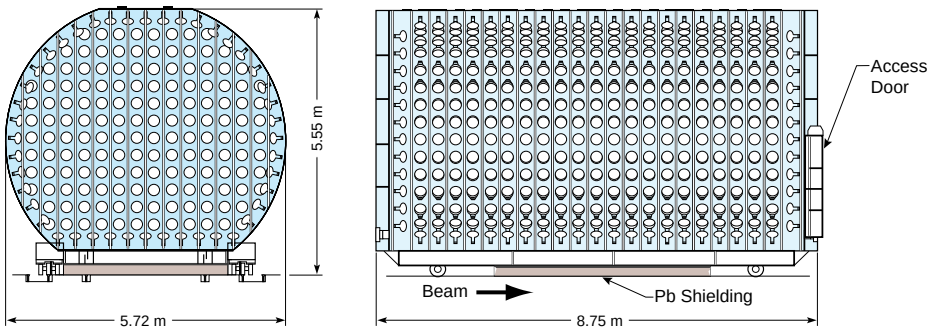

Fig. 13. Schematic representation of the LSND detector vessel and the photomultipliers pointing inward.

Michel electrons. Hence, the signal involves a prompt relativistic energy above threshold exhibiting the topological features of a positron, later followed by a signal characteristic of the neutron-capture photon. Information from the PMTs permits the reconstruction of the positron momentum, position of interaction, and associated times.

5.3. Data Selection

The experimenters [43] use a goodness-of-fit parameter (R) for each event, incorporating measurements of the various energies, times, and topological properties. Values with $R > 30$ are deemed likely to be signal. The expected background is of three general categories: (a) cosmic rays, uncorrelated with the beam; (b) beam-related events with an accidental photon; (c) beam related events with a correlated neutron. The first category is monitored directly with more than an order-of-magnitude more data taken during part of the time (94%) while the beam is off. The second category (b) is also monitored from data. The last category (c) includes, for example, rare production by an energetic antineutrino ($\bar{\nu}_\mu + p \rightarrow \mu^+ + n$) followed by prompt decay of the muon to a positron. All such backgrounds must be simulated with Monte Carlo calculations. Table 12 gives the numbers of events without and with a cut in the R parameter for events with energies $36 < E < 60$ MeV.

Note that an excess of high energy events exists even before any quality cuts are applied. After application of cuts, the excess 17.4 events has a

Table 12
The excess events from the LSND experiment with $36 < E < 60$ MeV. Shown are the selection (B) of the LSND paper [43].

$R >$	Signal	Beam Off	ν background	Excess
0	300	160.5 ± 3.4	76.2 ± 9.7	63.3 ± 20.1
30	22	2.5 ± 0.4	2.1 ± 0.4	17.4 ± 4.7

Poisson probability quoted as 4×10^{-8}. The electron energy distributions for events without and with the cut in R are shown in figure 14. In the upper plot, expected to be primarily background, the data points at lower energy appear similar to the background prediction (dotted histogram), and there is some excess at higher energy. The lower plot, after the selection on the event quality, R, shows many fewer events. The data at the higher energies clearly do not reproduce the dotted background histogram.

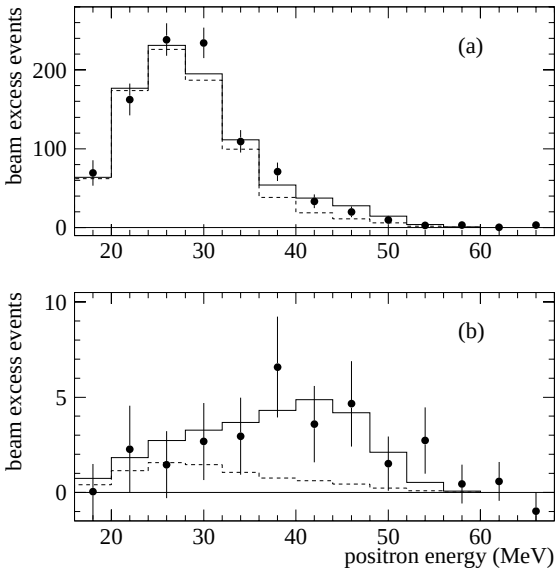

Fig. 14. The energy distribution of the LSND data shown as points for (a) no selection on the topology ($R > 0$) and (b) with $R > 30$. The dotted histogram is the predicted total for all known backgrounds. The full histogram is the prediction including background and hypothesized oscillations with the best fit parameters.

5.4. Oscillation Interpretation

The excess in figure 14b might be attributed to oscillations of $\nu_\mu \to \nu_e$. * A fit to the R-distributions of data and background in the range, $20 < E < 60$ MeV, provides an estimate of net excess in this expanded energy region of $51.8^{+18.7}_{-16.9}$ events, corresponding to an overall oscillation probability,

$$\mathcal{P}(\nu_\mu \to \nu_e) = (0.31^{+0.11}_{-0.10} \pm 0.05) \times 10^{-2}. \tag{5.3}$$

This two component oscillation hypothesis applied to the various variable distributions delineates the parameter space specified in figure 15. The darker area is the region with 90% likelihood (where the change in likelihood relative to the maximum value is $\Delta \log(\mathcal{L}) = 2.3$ units) and the light region is for 99% likelihood (where $\Delta \log(\mathcal{L}) = 4.5$ units). The other curves correspond to limits set by other experiments, wherein the parameter space above and to the right of the curves is forbidden.

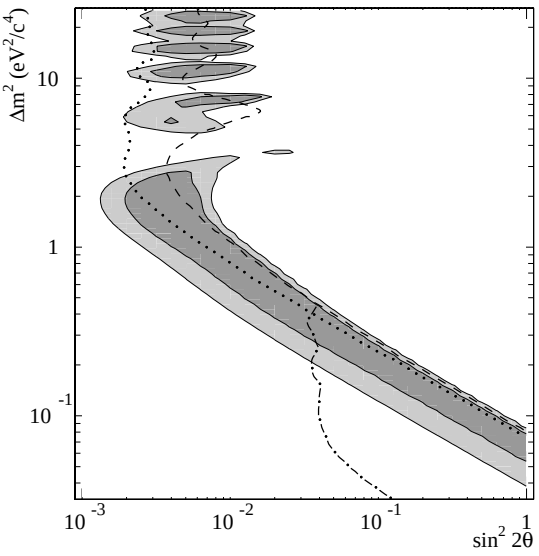

Fig. 15. Parameter space defined by the LSND detection of an anomalous number of electron neutrinos interpreted as oscillating from muon neutrinos. The regions and other curves are described in the text.

* As described earlier, antineutrinos are produced. We assume CP-invariance, so that particle and antiparticle transitions are equivalent.

The dot-dash curve is the limit from the Bugey reactor experiment [46]. The dotted curve shows the limit [47] from a Brookhaven experiment (E776) on limits of $\nu_\mu \to \nu_e$. The dashed curve shows the 90% confidence limits set by the KARMEN experiment at ISIS, discussed in section 5.6 [48]. Taking the LSND data and the various exclusions literally, there remains an allowed sliver in parameter space extending in $(\Delta m^2, \sin^2 2\theta)$ from $(2.0, .002)$ to $(0.3, .03)$.

5.5. LSND In-Flight Data

Recent corroboration has come[49] from the LSND collaboration. The experiment was operated with additional thin targets (in addition to those shown in figure 12) located 100 m and 135 m, respectively, upstream of the detector center. This geometry allows pions to decay in flight, extending the neutrino propagation distance for ν_μ flux with energies up to 300 MeV. The beam has only small contaminations of ν_e. The ν_μ flux is estimated to about 15% precision. The collaboration seeks ν_e interactions at higher energies, $60 < E_e < 200$ MeV, with little or no activity in the veto system, no activity before or after the event time, and an electron-like track identified using both scintillation and Ĉerenkov light. The increase in the parameters L and E is about a factor 3 - 4 in each. Hence, if the anomaly reported by the LSND decay-at-rest experiment were oscillations, this decay-in-flight experiment should observe a similar oscillation probability.

The experiment identified 23 events with a net estimated background of 12.5 events. (This corresponds to a Poisson probability of 6.0×10^{-3}.) If the excess is ascribed to a neutrino oscillation, the corresponding oscillation probability is

$$\mathcal{P}(\nu_\mu \to \nu_e) = (0.26 \pm 0.13 \pm 0.05) \times 10^{-2}$$

consistent with the probability from the decay-at-rest experiment given in equation (5.3). The parameter space defined by this measurement overlaps well with that shown in figure 15. The error is considerably larger than the decay-at-rest experiment, but it must be acknowledged to be a welcome corroboration.

5.6. Other Accelerator Information...KARMEN

There are several other experiments which bear on the LSND anomaly. The Brookhaven experiment[47] placed strong limits on the oscillation parameter space covered by LSND, but it does not exclude all possibilities. The KARMEN experiment [48] is very similar in concept to LSND.

KARMEN operates[50] with an 800 MeV proton beam from the ISIS accelerator at Rutherford laboratory. The neutrino spectrum originates from the same kind of stopping pion/muon source as the LSND decay-at-rest experiment; however, the detector mass is smaller (56 tons versus LSND 176 tons) and the distance to the source is smaller (17.6 m versus LSND 30 m). This shorter distance increases solid angle (and flux), but decreases sensitivity at small Δm^2. (See section 3.3.) The detector uses liquid scintillator for good energy resolution on detected electrons; paper coated with Gd_2O_3 detects the thermalized neutrons. The experiment utilizes a short duty cycle and short pulses for good time resolution. The best present sensitivity comes from seeking the transition $\bar{\nu}_\mu \to \bar{\nu}_e$, for which KARMEN sees a small excess (considered not statistically significant). They obtain a (90% CL) limit of $\mathcal{P} < 0.0085$ which is not in conflict with the LSND observations, both because this probability is larger than that reported by LSND in equation (5.3) and because the experimental geometry is different.

The KARMEN version of the current situation, shown in figure 16, is similar to the LSND version in figure 15. Major shielding improvements and running for two additional years should provide KARMEN with substantially improved data. If there are no oscillations, the dashed 90% CL exclusion curve labeled $\mathcal{P} = 0.001$ indicates the expected sensitivity. Hence, if no signal were observed, the 90% CL KARMEN exclusion region might extend down to just reach the outer edge of the included 99% CL LSND region.

5.7. Reactor Experiments

One exclusion curve in figure 16 is the limit placed by a recent reactor experiment, BUGEY. This limit clearly states that the LSND anomaly, if oscillations, does not involve the region at large $\sin^2 2\theta$ and small Δm^2.

Reactor experiments use profuse numbers of $\overline{\nu}_e$ produced by power reactors. The typical flux is 2×10^{20} neutrinos per gigawatt of produced power. The neutrinos are detected using the reaction $\overline{\nu}_e + p \to e^+ + n$. Either the positron or both the positron and the neutron are detected. After long operation, such experiments are limited by the precision of the normalized flux, typically several percent. Table 13 [51] shows the progression in sensitivity for such experiments over many years.

At this time, the CHOOZ experiment is taking data and the Palo Verde experiment is preparing to do so. These experiments will extend the search for transformation of electron neutrinos at large mixing down to mass pa-

rameters with $\Delta m^2 > .001$ eV^2 in the near future.* This will cover even more of the region of large mixing delineated by the LSND anomaly. It should also clarify whether the oscillation interpretation of the atmospheric anomaly permits $\nu_\mu \to \nu_e$ or not.

5.8. Conclusions

The anomaly reported by the LSND experiment is neither confirmed nor contradicted by other experiments. The LSND collaboration has performed an experiment using in-flight decays; this result corroborates the effect. Limits from the reactor experiments already make it unlikely that the parameter space at large $\sin^2 2\theta$ is involved. New information is expected in the near future by continued operation of LSND and KARMEN. In the longer term, there is a proposed experiment [53] at Fermilab (BOONE) which will explore (and extend) this region using neutrinos created by the

* Note added in proof: Results announced in November 1997 by the CHOOZ Collaboration [52] exclude mixing of electron antineutrinos with full mixing for $\Delta m^2 > 0.9 \times 10^{-3}$ eV^2.

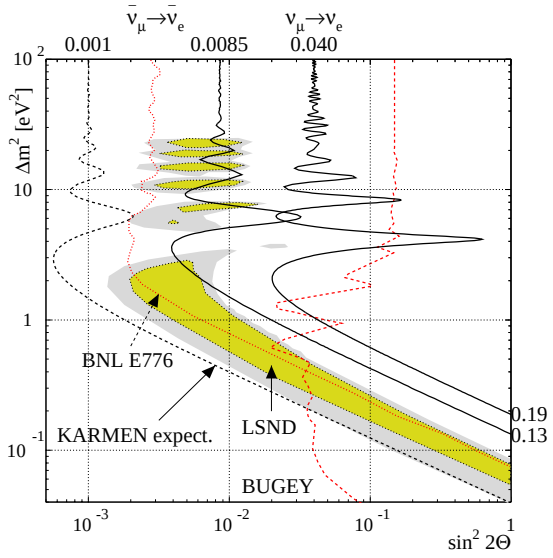

Fig. 16. KARMEN limits. The LSND allowed region is shown shaded. The present KARMEN exclusion curve for $P < .0085$, as shown, excludes only portions of the region at larger mass. At such masses, the older BNL limit is more stringent. See text.

8 GeV booster. Also being discussed is a new experiment at the proposed European Spallation Source.

6. Future and End

6.1. Introduction

Over the past few days, we have reviewed experimental neutrino measurements that do not conform to our expectations: the Solar, Atmospheric, and LSND effects. It is exciting to have data to stimulate our imaginations and point us in a direction. Please be aware that there are many experiments completed, in operation, and planned that we have not discussed, simply because these do not report anomalies suggesting oscillations or their limits are not directly applicable to parameters for which anomalies *are* reported. I encourage the student to read about *all* the experiments [54,55]. They form the backbone of the field.

6.2. Neutrino Anomalies

Each of the three unexpected results deserves the attribution of "anomaly". Each has been obtained from carefully executed experiments. There are differing levels of corroboration among them, as described previously. None of the three anomalies *must* be due to neutrino oscillations. However, hints are strong enough to consider seriously the implications of this interpretation.

The Atmospheric and LSND anomalies require larger values of Δm^2 than needed to explain the Solar anomaly. This upper region of parameter space

Table 13
Progress in reactor experiment sensitivity.

Experiment	Tgt Mass	L (max)	Δm^2
Grenoble	320 kg	8.75 m	0.15 eV^2
Savannah River	260 kg	24.0 m	0.05 eV^2
Gösgen	320 kg	65 m	0.019 eV^2
Krasnoyarsk	600 kg	92 m	0.014 eV^2
Rovno	200 kg	25 m	0.06 eV^2
Krasnoyarsk	600 kg	230 m	0.01 eV^2
Bugey III	1200 kg	230 m	0.01 eV^2
Palo Verde	12000 kg	800 m	$\sim 10^{-3}$ eV^2
Chooz	4800 kg	1025 m	$\sim 10^{-3}$ eV^2

for each of the three flavor transitions is shown from a recent review [55] in figure 17. The "interesting" regions are shown shaded. More recent limits from the CHOOZ experiment[52] make it unlikely that the Atmospheric anomaly involves $\nu_\mu \to \nu_e$.

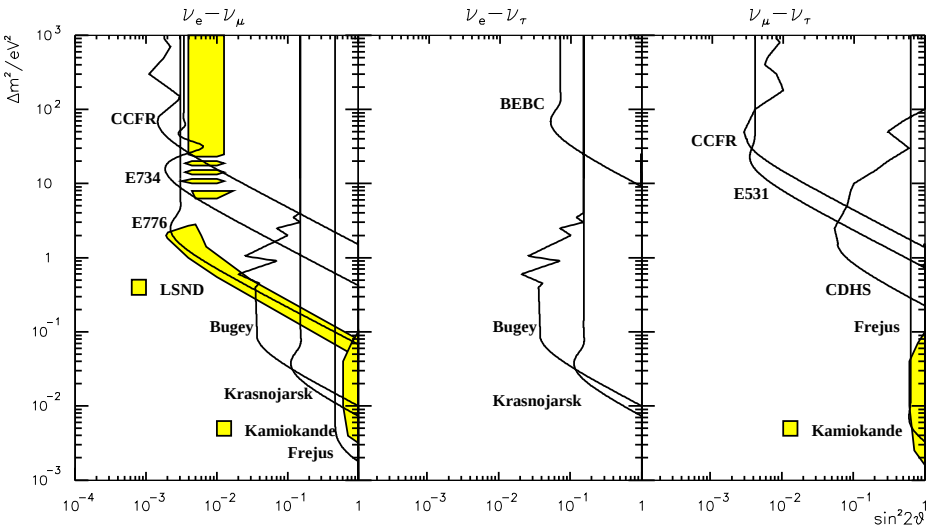

Fig. 17. Summary of oscillation parameter regions indicated by the Atmospheric and LSND anomalies.[55] See text.

To place *all* the anomalies into perspective, look at the alternative parameter sets (at order of magnitude precision) describing the three anomalies tabulated in table 14. These very approximate regions specified by the experimental anomalies are not explicitly disallowed by limits set by other experiments (with the MSW interpretation taken for Solar).

Table 14
Summary of oscillation parameters.

Type	$\Delta m^2\,(eV^2)$	$\sin^2 2\theta$	Transition
Solar - MSW	10^{-5}	10^{-2} & 0.7	$\nu_e \to \nu_\mu,\, \nu_\tau,\, \nu_x$
Atmospheric	10^{-2}	1	$\nu_\mu \to \nu_\tau,\, \nu_x$
LSND	$10^{-1} - 10^{+1}$	10^{-2}	$\nu_\mu \to \nu_e$

The parameter space is further summarized in figure 18, which is a (crude personally sketched) cartoon of the available parameter space (shaded and labeled) for two-component oscillation interpretation of the three different anomalies, with the Solar anomaly taken *a la* MSW.*

6.3. Can All Anomalies be Oscillations?

Though we have ingredients for several different kinds of oscillations, and this is a possible interpretation, it seems unlikely that all these anomalies are due to oscillations. If we restrict ourselves to the three (and only three) flavors associated with low mass left-handed neutrinos, then the sum over the mass parameters must be zero, $\sum \Delta m^2 = 0$, as described in section 3. For the three mass parameters delineated above, this sum is

$$(0.1 - 10) \pm (0.01) \pm (10^{-5}) \stackrel{?}{=} 0$$

taking the mass parameters in the order: LSND, Atmospheric, and Solar. There is simply no way that these three can be a closed set describing oscillations among only the three known flavors. This is borne out by efforts to quantitatively reconcile all three sets of parameters to three flavors.[56]

If all the anomalies represent oscillations, therefore, at least one additional sterile flavor must exist. This is a possibility, but in my opinion the present data do not yet *demand* such an explanation. It is difficult, as an experimentalist, to conclude that there are sterile flavors when we have not yet demonstrated that any of the anomalies must be oscillations.

To make progress, it is extremely important for currently planned and operating experiments [54,55] to expeditiously collect and analyze data. If the anomalies can be corroborated, the likely range of parameter space will be more clearly delineated. If new data contradict previous evidence, this fact might keep us from mounting time-consuming and costly experiments to accomplish the same result, or to permit those experiments to explore more interesting parameter ranges.

6.4. Demonstrating Oscillations

The anomalies have given us important clues that may lead to the discovery of neutrino oscillations. The most important experimental problem now is to clearly demonstrate that oscillations are indeed happening. How does

* For vacuum oscillations, Δm^2 is even lower by five orders of magnitude (with large mixing). Also, only the "small mixing angle" for the MSW solution is shown in the figure.

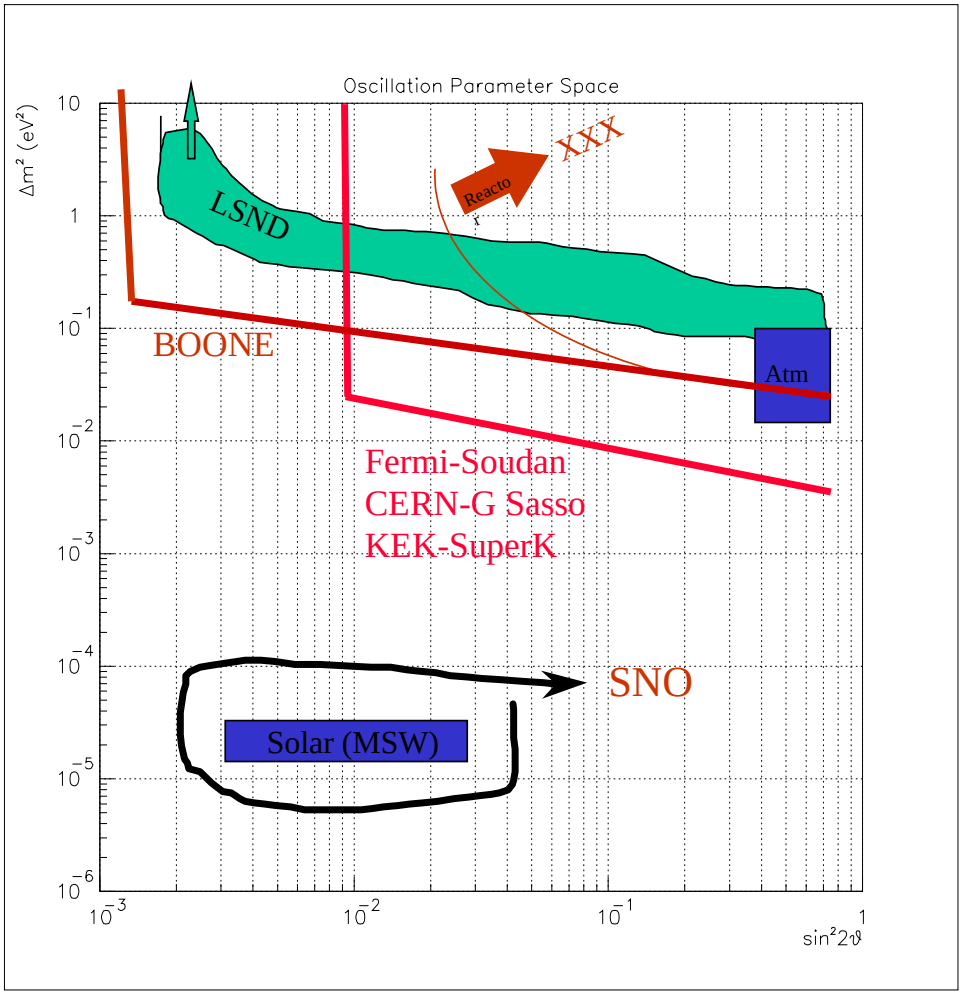

Fig. 18. Cartoon of the interesting oscillation parameter regions delineated by the existing anomalies.

one demonstrate oscillations? At the risk of sounding simplistic, I suggest the best way to show that a parameter oscillates is to actually see data go up and down when plotted against the parameter! This will not always be an easy task. Ultimately this is a requirement, but we must first find

natural next steps.

At Higher Δm^2

Data are required to delineate clearly the alternatives and, if oscillations *do* exist, ultimately prove this – and then carefully measure the parameters. Many experimental groups are gearing up to do just this. Fortunately, Δm^2 values associated with the Atmospheric and LSND anomalies are large enough to be amenable to test with controlled accelerator experiments. The (crudely sketched) limits of figure 18 shows a sampling of experiments expected to attack this goal at high values of the mass parameter in the near future.

BooNE, an experiment[53] proposed to use the 8 GeV booster at Fermilab, should completely explore the parameter space specified by LSND. The experiment would use a technique similar to that used by LSND, with much higher rates.

Many groups are considering ways to explore the region specified by the Atmospheric anomaly. Programs are in various stages of consideration and preparation at CERN, Fermilab, and KEK accelerator facilities. In order to cover the interesting mass region, however, the detectors must be located some distance from the accelerators. At CERN and Fermilab, the detectors would be about 730 km way. From CERN, neutrinos would travel to detectors in the Italian Gran Sasso; from Fermilab, to the Soudan Mine in Minnesota. The MINOS program at Fermilab has been approved and some construction is currently underway. Both laboratories would need to construct new beam lines to extract the accelerated protons, target them, and direct the neutrinos in the appropriate direction.

At KEK, a good detector of beam-generated neutrinos (SuperKamiokande) already is situated 250 km from KEK. A proton beam from the 12 GeV accelerator needs to be extracted and targeted in the appropriate direction. Plans are underway to do just this. A future proposed 50 GeV proton accelerator at KEK would provide an even better neutrino beam to explore the region delineated by the Atmospheric anomaly.

As sketched in figure 18, these programs should cover the Atmospheric region unless the interesting parameter space shifts considerably with more information. It is very important to delineate that region clearly ... only SuperKamiokande operating with atmospheric neutrinos can do this now. Preliminary data [22] corroborates the overall effect; but the mass region tentatively specified by Kamiokande zenith angle data has not yet been corroborated. The expensive long baseline experiments will need a very specific target. (Excuse the pun!)

At Lower Δm^2 - SNO

From figure 18 and table 14, we see that the Solar anomaly suggests regions of Δm^2 which are smaller by at least a factor of 10^{-3}. This means that a facility-based neutrino experiment would need to use neutrinos three orders of magnitude less energetic, or be located three orders-of-magnitude further, or some combination. Furthermore, the presently preferred MSW solution has a very small mixing angle. It appears unlikely that these parameter regions will be explored using terrestially generated neutrinos.*

Hence, the circled Solar parameter space in the lower part of figure 18 presents a formidable challenge. A very important experiment, gearing up to take data beginning next year, will respond to this challenge. If successful, we will come a long way toward demonstrating oscillation of Solar neutrinos.

The Sudbury Neutrino Observatory (SNO) is located [57] in the Creighton Mine in Sudbury, Canada. The construction is nearly complete; filling of the detector should begin over the next few months. The object is to detect the higher energy neutrinos from the Sun interacting in a heavy water (D_2O) target. The 1000 tons of target are enclosed in a transparent sphere and surrounded by 7000 tons of light water, which itself is surrounded by 10,000 photomultiplier tubes covering 56% of the area. The detected reactions include

$$\begin{array}{ll} CC: & \nu_e + D \rightarrow e^- + p + p \\ NC: & \nu_x + D \rightarrow \nu_x + n + p \end{array} \tag{6.1}$$

as well as the purely leptonic process, $\nu_x + e^- \rightarrow \nu_x + e^-$. These reactions have well-known cross sections; measured rates give unambiguous measures of flux. The CC process can only be initiated by electron-type neutrinos; the NC process occurs from all neutrinos whatever their flavor when they encounter the target. (As a further check, the leptonic process occurs with all flavors, but is six times more likely from electron flavored neutrinos.)

Detection of these processes is a nontrivial task. The CC process requires observation of the low energy electron – such electrons have been observed in the Kamiokande detectors. But the NC process requires observation of a low energy neutron in the final state, and nothing else. The experimenters have alternative techniques for achieving this. For SSM ν_e fluxes, the CC process is expected at a rate of about 7000 events per year and the NC rate is about 2000 events per year. The threshold energies

* The large mixing MSW solution could conceivably be probed using neutrinos from power reactors located some fraction of the world away. Even this, though conceivable, looks very difficult.

for the NC and CC processes are a few MeV; for detection in SNO, the neutrinos would need to be above about 5 MeV. Hence the upper part of the neutrino spectrum is sampled: the region where the flux from the ^8B cycle dominates.

The two detected processes in 6.1 will provide from a single detector independent measures of the total neutrino flux (all flavors) and the electron-flavor neutrino flux. The SNO experiment, therefore, has the potential to tell us that neutrinos at the upper end of the Solar spectrum have changed their flavor between production at the Solar core and detection on Earth. We look forward to SNO results with excitement.

6.5. Conclusions

Finding neutrino oscillations with new parameter values requires new experiments. Many experiments are operating or are planned to explore regions previously unexplored. [54,55]

The LSND and Atmospheric anomalies provide important hints of neutrino oscillations. The parameter spaces delineated by these require further exploration. Some experiments are still in operation. Others are planned to explore these regions: (1) Future long baseline neutrino beams are planned or are in construction at Fermilab and KEK to explore the Atmospheric parameter space. The BOONE experiment proposed for Fermilab should explore the LSND parameter space.

The Solar anomaly, indicative of a much smaller mass parameter (and possibly smaller mixing parameter) represents a substantial experimental challenge if oscillations are the underlying reason for the anomaly. Laboratory experiments will not easily cover the interesting parameter spaces. The SNO experiment, to begin operation soon, will make measurements of total and electron neutrino flux at the upper end of the Solar spectrum. If oscillations are indicated by SNO, it will be essential to extend this technique to lower energies.

Experimental observation of oscillations between neutrino flavors would demonstrate that neutrinos have finite mass and that leptonic flavor is not conserved in all interactions. Between pursuing resolutions of existing anomalies and opening of new parameter space, we hope that definitive evidence for oscillations will be seen. Conclusive evidence for neutrino mass and mixing would provide an intellectual leap. Most needed is for people like the students at this school to provide new ideas and energy in exploring future experimental steps. My advice is, "CHARGE!"

6.6. Acknowledgements

The school organizers, staff, lecturers, and students deserve my resounding, "Thank you!" for a stimulating and warm visit to Les Houches. Though I retain responsibility for all errors, these lectures have benefited from many discussions with colleagues and friends. These include E. Beier, J. Conrad, N. Christ, M. Diwan, M. Goodman, M. Kamionkowski, S. Ritz, M. Shaevitz, L. Wai, and K. K. Young. Technical assistance on postscript and latex from M. Seman and W. Seligman is gratefully acknowledged. Special thanks to Marc Kamionkowski, Steve Ritz, and Ann Therrien for suggestions regarding the final manuscript.

References

[1] G. S. Abrams, et al, Phys. Rev. Lett. 63 (1989) 2780.
[2] Particle Data Group, Rev. Part. Phys. 54 (1996) page 23 and LEP references on page 189.
[3] P. Langacker and S. U. Sankar, Phys. Rev. D40 (1989) 1569.
[4] See, for example S. R. Mishra and F. Sciulli, Ann. Rev. Nucl. and Part. Sc. 39 (1989) 259;
L. Wai, "Search for a 100 GeV Mass RH Neutrino at HERA ...", PhD thesis Columbia University (1995);
J. Breitweg, et al, Z. Phys. C76 (1997) 631.
[5] S. Adelberger, et al, Proceedings of the 1994 Snowmass Summer Study, Particle and Nuclear Astrophysics and Cosmology in the Next Millenium (World Scientific, 1994) p 195;
P. Langacker, et al, Particle Physics Perspectives and Opportunities (World Scientific, 1995) p. 127.
[6] J. Brunner, "Experimental Results On Neutrino Masses And Lepton Mixing", Neutrino '96 (CERN-PPE-97-038, Apr 1997). Published in Fortsch. Phys. 45 (1997) 343.
[7] T. J. Loredo and D. Q. Lamb, Proceedings of Conference on Relativistic Astrophysics (Dallas 1988), p. 601.
[8] K. Hirata, et al., Phys. Rev. Lett. 58 (1987) 1490.
R. M. Bonita et al., Phys. Rev. Lett. 58 (1987) 1494.
[9] G. Raffelt, "Neutrino Masses in Astrophysics and Cosmology" (Zuoz Summer School, 1996) page 69 (hep- ph/9704315).
[10] For very readable descriptions of the Dirac and Majorana properties of neutrinos see, for example, the reviews by B. Kayser and S. P. Rosen in *Massive Neutrinos in Astrophysics and in Particle Physics,* - Proceedings of the Fourth Moriond Workshop, La Plagne, Savoie, France, 1984).
[11] F. Avignone, Proceedings of the 1994 Snowmass Summer Study, Particle and Nuclear Astrophysics and Cosmology in the Next Millenium (World Scientific, 1994) page 215.
[12] A. Rubbia, reported at the Lepton-Photon Conference (Hamburg 1997).

[13] P. Langacker, R. Rameika, and H. Robertson, Particle Physics Perspectives and Opportunities (World Scientific, 1995) p. 127.
[14] S. A. Bludman, D. C. Kennedy, and P. Langacker, Nucl. Phys. B374 (1992) 373; Phys. Rev. D45 (1992) 1810; and quoted references.
[15] J. N. Bahcall, Neutrino Astrophysics (Cambridge University Press, Cambridge) 1989.
[16] N. Hata and P. Langacker, "Solutions to the Solar Neutrino Anomaly", Phys. Rev. D56 (1997) 6107 [hep-ph/9705339]. Previous and original references are described in this paper.
[17] J. N. Bahcall and M. H. Pinsonneault, Rev. Mod. Phys. 67 (1995) 781.
[18] W. C. Haxton, K. Lande and S. P. Rosen, "Solar Neutrinos", Proc. of 1994 Snowmass Summer Study Particle and Nuclear Astrophysics and Cosmology in the New Millenium, page 235.
[19] J. N. Bahcall, K. Lande, R. E. Lanou, J. Learned, R. G. H. Robertson, and L. Wolfenstein, Nature 375 (1995) 29- 34 and IASSNS-AST-95-20 (Mar 1995).
[20] Till A. Kirsten, "Results From Solar Neutrino Experiments", http://kosmopc.mpi-hd.mpg.de/GALLEX/ROM.HTML.
[21] K. S. Hirata, etal, Phys. Rev. Lett. 65 (1990) 1301; 66(1991) 9; Phys. Rev. D44 (1991) 2241.
[22] Y. Totsuka, "Non-accelerator Neutrino Physics", Proceedings of the 1997 Lepton Photon Conference (Hamburg 1997).
[23] Kamiokande: K. Hirata, et al., Phys. Rev. Lett. 58 (1987) 1490.
IMB: R. M. Bonita, et al, Phys. Rev. Lett. 58 (1987) 1494.
[24] K. K. Young and L. Wai (U of Washington), private communication.
[25] P. Langacker, "Solar Neutrinos", 32nd Int'l School of Subnuclear Physics, Erice (July 1994). U. of Penn. UPR0640T.
[26] S. Turck-Chièze and I. Lopes, Astrophys. J. 408 (1993) 347. S. Turck-Chièze, S. Cahen, M. Cassè, and C. Doom, Astrophys. J. 335 (1988) 415.
[27] J. N. Bahcall, Sarbani Basu, Pawan Kumar, Astrophys.J. L91-L94 (1997) 485 [astro-ph/9702075]
J. N. Bahcall, astro-ph/9702057.
[28] F. Hill, et al. Science 272 (1996)1292;
A.G. Kosovichev, et al Sol. Phys. (to be published);
J. Christensen-Dalsgaard, astro-ph9702094.
[29] Y. Fukuda, et al, Kamioka III Collab, Phys. Rev. Lett. 77 (1996) 1683.
[30] A. Romosan et al. (CCFR Collab) Phys. Rev. Lett. 78 (1997) 2912 [hep-ex/9611013].
[31] L. Wolfenstein, Phys. Rev. D17 (1978) 2369; Phys. Rev. D20 (1979) 2634. S.P. Mikheyev and A. Yu. Smirnov. Sov. J. Nucl. Phys. 42 (1986) 913; Nuovo Cimento C9 (1986) 17.
[32] L. Wolfenstein, Neutrino '86 (Tohumku U.) p 1.
[33] G. Gelmini and E. Roulet, "Neutrino Masses" Rept. Prog. Phys. 58 (1995) 1207 [hep/ph9412278].
[34] See, for example, S.M. Bilenky, et al, "Constraints on Long-Baseline Neutrino Oscillation Probabilities and CP Asymmetries from Neutrino Oscillation Data", hep-ph/9705300, and references therein.
[35] G. Barr, T. K. Gaisser, and T. Stanev, Phys. Rev. D39 (1989) 3532.
[36] M. Honda, et al, Phys. Lett. B248 (1990) 193.
[37] E. V. Bugaev and V. A. Naumov, Phys. Lett. B232 (1989) 391.
[38] T. K. Gaisser, "Review of Atmospheric Neutrinos", presented at 17th International

Conference on Neutrino Physics and Astrophysics (Neutrino 96), Helsinki, Finland, 13-20 Jun 1996 [hep-ph/9611301].
[39] O. Perdereau (Frejus) "Final Results Of The Frejus Proton Decay Experiment On Atmospheric Neutrinos" presented at Tests of Fundamental Laws in Physics: Rencontre de Moriond, Les Arcs, France, Jan 26 - Feb 2, 1991. Published in Moriond Workshop 1991:117-122
[40] Y. Fukuda, et al, Phys. Lett. B335 (1994) 237.
[41] G. L. Fogli and E. Lisi, Phys Rev D52 (1995) 2775 [hep-ph9504287].
[42] K. Daum, et al, Z. Physik C66 (1995) 417.
[43] C. Athanassopoulos, et al, Phys. Rev. Lett. 77 (1996) 3082.
[44] C. Athanassopoulos, et al, Phys. Rev. C54 (1996) 2685.
[45] C. Athanassopoulos, et al, Nucl. Instrum. Meth. A388 (1997) 49.
[46] B. Achkar, et al., Nucl. Phys. B434 (1995) 503.
[47] L. Borodovsky et al., Phys. Rev. Letters 68 (1992) 274.
[48] B. Bodmann et al, Phys. Lett. B267 (1991) 321; B. Bodmann et al, Phys. Lett. B280 (1992) 198; B. Zeitnitz, et al Prog. Part. Nucl. Phys. 32 (1994) 351.
[49] C. Athanassopoulos et al, UCRHEP-E-191, June 1997 [nucl-ex/970600], submitted to Phys. Rev. C.
[50] Klaus Eitel, "KARMEN: Present Neutrino Oscillation Limits and Perspectives After The Upgrade", Presented at 32nd Rencontres de Moriond: Electroweak Interactions and Unified Theories,Les Arcs, France, 15-22 Mar 1997 [hep-ex/9706023].
[51] H. de Kerret, et al., "Proposal to Search for Neutrino Vacuum Oscillations to $\Delta m^2 = 10^{-3}$ eV^2 Using a 1 km Baseline Reactor Neutrino Experiment", June 1993.
[52] M. Apollonio, et al. "Initial Results from the CHOOZ Long Baseline Reactor Neutrino Oscillation Experiment" [hep- ex/9711002].
[53] J. Conrad, W. Louis, et al, "A letter of intent to measure oscillations disappearance at the Fermilab Booster: BooNE", May 1997.
[54] For a very useful WWW description of ongoing experiments, see M. Goodman, et al, http://www.hep.anl.gov/NDK/Hypertext/nu_industry.html
[55] J. Brunner, Fortsch. Phys. 45 (1997) 343 [CERN-PPE/97-38].
[56] G.L.Fogli, et al, [hep-ph/9706230];
C. Y. Cardall and G. M. Fuller [astro-ph/9606024].
[57] H. H. Chen, et al, Phys. Rev. Lett. 55 (1985) 1534;
G. Aardsma et al., Phys. Lett. B194 (1987) 321;
G. T. Ewan et al., Sudbury Neutrino Observatory Proposal SN-87-12 (1987).